



HAL
open science

The original and impactful exploitation of chemical energy in heat pumps

Aya Barakat, Silvia Lasala, Philippe Arpentinier, Jean-Noël Jaubert

► To cite this version:

Aya Barakat, Silvia Lasala, Philippe Arpentinier, Jean-Noël Jaubert. The original and impactful exploitation of chemical energy in heat pumps. *Chemical Engineering Journal Advances*, 2022, 12, pp.100400. 10.1016/j.cej.2022.100400 . hal-03788500

HAL Id: hal-03788500

<https://hal.science/hal-03788500>

Submitted on 26 Sep 2022

HAL is a multi-disciplinary open access archive for the deposit and dissemination of scientific research documents, whether they are published or not. The documents may come from teaching and research institutions in France or abroad, or from public or private research centers.

L'archive ouverte pluridisciplinaire **HAL**, est destinée au dépôt et à la diffusion de documents scientifiques de niveau recherche, publiés ou non, émanant des établissements d'enseignement et de recherche français ou étrangers, des laboratoires publics ou privés.



Distributed under a Creative Commons Attribution 4.0 International License



The original and impactful exploitation of chemical energy in heat pumps

Aya Barakat^a, Silvia Lasala^{a,*}, Philippe Arpentinier^b, Jean-Noël Jaubert^a

^a Université de Lorraine, Laboratoire Réactions et Génie des Procédés, 54000 Nancy, France

^b Air Liquide, Innovation Campus Paris, 1 chemin de la porte des loges, 78354 Jouy-en-Josas, France

ARTICLE INFO

Keywords:

Heat pump
Reactive working fluid
Reverse Brayton cycle
Thermochemistry
Ideal gas mixture
Sustainability

ABSTRACT

In light of reducing carbon emissions and the tension on non-renewable energy sources, heat pumps are being investigated as an alternative to fossil-fuel-dependent energy converters in heat demanding applications. On the basis of the impactful results the authors obtained in previous research around the potential of using reactive fluids—instead of inert ones—as novel working fluids in power cycles, the study has been extended to heat pump systems. The thermodynamic analysis of heat pumps operating with reactive gases as working fluids is thus the objective of the present work. More specifically, the analysis is based on the use of instantaneously equilibrated fictive gaseous reactions, with the aim to thoroughly assess the impact of different stoichiometries and thermochemical characteristics of chemical reactions. This studied heat pump is based on the reverse Brayton cycle. Furthermore, the behavior of the fluid in each unit operation of the cycle is investigated and all the results are compared to those of a heat pump utilizing comparable inert fluids; that is to preliminarily quantify the potential gains in performance. For the considered spectrum of reactive fluids, operating conditions, and reaction stoichiometries, the corresponding results show a range of potential reactive fluids that can be utilized in heat pumps and reveal an increase of more than 200% in the system's coefficient of performance compared to inert-fluid heat pumps.

1. Introduction

Heating is the largest global energy use. According to the International Energy Agency (IEA) [1], heating provided for residences, industrial processes, and other applications accounted for around 50% of the global energy consumption in 2021. Fossil-fuel based heating equipment, such as coal, oil, and gas boilers, dominated the global sales until 2020 (market share greater than 50%). However, a transition towards greener or more efficient technologies has been promoting systems like heat pumps (HP) and renewable heating equipment, and the market share of these technologies has been slowly yet steadily growing. In 2021, HPs were meeting only around 7% of the global building heating demand [2]. However, the IEA demonstrates that, in order to meet the net zero emissions by 2050 scenario, the installed HPs should increase from 180 million (current) to 600 million by 2030.

A HP is a thermodynamic cycle which absorbs heat from a heat source, upgrades this heat, and transfers it to a heat sink using compression work. HP systems can be a greener alternative to fossil-fuel based heating technologies by upgrading low quality heat to a higher quality one, especially in low-temperature waste heat recovery (WHR)

applications [3–5]. In fact, HPs provide 2.5 to 11 times more useful energy compared to other WHR systems for the same waste heat input, in the context of low-temperature WHR applications [4,6]. Furthermore, in line with the net zero emissions target, several countries are concentrating their efforts to motivate residents to switch to HP technologies in order to meet their space and water heating needs. In the United States, the share of HPs for the heating of new buildings is around 50% [2]. Furthermore, other countries like Canada and China are devoting efforts to encourage the installation of HP systems for space heating by offering subsidies to their citizens [2,7]. Moreover, techno-economical surveys have been recently financed by the Government of the Russian federation to identify the most suitable city to install air source and ground-source heat pumps [8].

However, there are still barriers limiting the wider commercialization of HPs. These include the high initial costs, limited availability of high-temperature-range refrigerants that have low global warming potential (GWP), immature technology, limited energy performance, and the competing fossil-fuel-dependent heating technologies [9,10].

Pertaining to the energy performance, improving the performance of a heat pump is carried out by selecting the favorable system technology (vapor compression, absorption, and reverse Stirling HP), optimizing the

* Corresponding author: Dr. Silvia Lasala, Université de Lorraine, LRGP, 1 rue Grandville, 54000 Nancy, France
E-mail address: silvia.lasala@univ-lorraine.fr (S. Lasala).

Nomenclature			
A_m	Molecule of m fictive atoms A	T_H	Heat sink temperature
A_n	Molecule of n fictive atoms A	v	Specific volume
COP	Coefficient of performance	w_{comp}	Compression specific work
C_p	Specific heat capacity	WHR	Waste heat recovery
G	Total Gibbs energy of the system	W_{net}	Net work input to the heat pump system
GWP	Global warming potential	$w_{net,in}$	Specific net work input to the cycle
h	Specific enthalpy	w_{turb}	Turbine expansion specific work
$H_{i,pure}(T)$	Molar enthalpy of species i	z_i	Molar fraction of species i
HP	Heat pump	γ	Specific heat ratio $\gamma = C_p / C_v$
HTHP	High temperature heat pump	η_{II}	Second-law efficiency
IEA	International Energy Agency	μ_i	Chemical potential of species i
IHX	Internal heat exchanger	μ_i°	Chemical potential of pure ideal gas i at the standard pressure P°
K_{eq}	Equilibrium constant	v_i	Stoichiometric coefficient of species i
M	Molar mass of the working fluid (ideal gas mixture)	$\xi(T, P)$	Extent of reaction
M_i	Molar mass of species i	ρ	Density
\dot{m}	Mass flow rate	Δn	Variation in the total number of moles during a process (outlet minus inlet)
n_i	Number of moles of species i	ΔT_{H-C}	Temperature difference between the heat sink and source
$n_{i,0}$	Initial number of moles of species i	ΔT_{pp}	Pinch point temperature difference
n_{tot}	Total number of moles	$\Delta_f H_i^\circ$	Standard molar enthalpy change of formation of species i at the reference temperature T_0
n, m	Number of atoms of molecules A_n and A_m , respectively	$\Delta_R G$	Gibbs-energy change of reaction
ODP	Ozone Depletion Potential	$\Delta_R H^\circ$	Standard enthalpy of reaction
P	Pressure	$\Delta_R S^\circ$	Standard entropy of reaction
P°	Standard pressure (1 bar)		
Q_C	Heat absorbed from the heat source	Subscripts	
Q_H, \dot{Q}_H	Thermal power supplied to the heat sink	C	Cold (corresponding to the heat source)
q_H	Specific heat supplied to the heat sink	comp	Compression
R	Ideal gas constant	eq	Chemical equilibrium
r_p	Pressure ratio	H	Hot (corresponding to the heat sink)
s	Specific entropy	HX1	Heat sink side heat exchanger
$S_{i,pure}(T, P)$	Molar entropy of the pure ideal gas i	in	Inlet
$S_i^\circ(T_0)$	Standard molar entropy of species i at 1 bar and the reference temperature T_0	max	Maximum
T	Temperature	tot	Total
T_0	Reference temperature (25°C)	turb	Turbine expansion
T_C	Heat source temperature		

system configuration according to the operating conditions, and selecting the most suitable working fluid [11–13]. A HP configuration can be optimized by applying modifications such as adding an internal heat exchanger (IHX) [14], compression intercooling, vapor injection compression (multi-stage compression with a flash chamber) [15], and cascaded HP system [16]. Other studies aim to improve the efficiency of HP-based systems by acting on the integration of HPs with original systems, providing renewable heat to the heat pump through its evaporator [17]. On the other hand, several considerations must be accounted for when selecting the working fluid of the heat pump. Environmental compatibility (GWP [18] and ODP), price and availability of the fluid, safety group classification, thermophysical properties (compressor discharge and suction temperatures, critical point, volumetric capacity...), and compatibility with the materials of a HP are key factors to select a high-performing working fluid for a HP system [19].

Some commercially available industrial (high temperature) HPs provide temperatures in the range of 130°C to 165°C (SGH 165 HP from Kobe Steel) with heat capacities reaching 20 MW (Titan OM from Johnson Controls) [9]. These systems utilize modifications like IHXs to ensure superheating, economizer cycles, turbo compressors with intermediate vapor injection, parallel piston compressors, and two-stage cascade systems. Furthermore, the refrigerants used are mainly R245fa, R717, R744, R134a, and R1234ze(E). As for the coefficient of performance (COP) values, they lie within the range of 1.6 to 5.8 with a

temperature lift of 130°C to 25°C, respectively.

On the other hand, these high temperature heat pumps (HTHP) are still under study and development in order to improve the system's performance, find suitable environmentally-friendly refrigerants, and achieve high heat sink temperatures (above 100°C) [9]. Arpagaus et al. [9] in their review of HTHPs, assessed 17 HPs that are still in research status. The highest heat sink temperature achieved experimentally is 160°C (developed by the Austrian Institute of Technology, Vienna, Chemours, Bitzer) using the R1336mzz(Z) refrigerant and an IHX, with heating capacities that range from 1.8 kW to several 100 kW. In such experimental system, compression is mainly carried out in piston compressors, and most of these systems are single stage. The system modifications adopted include IHXs, economizer cycles, and compression with intermediate vapor injection. Only a few studies focus on two-stage cycles or cycles with subcoolers for combined water heating. Additionally, the refrigerants under study are mainly R1336mzz(Z), R718, R245fa, R1234ze(Z), R600, and R601, besides other fluids whose chemical composition is not published yet. As for the COP values, they lie within the range of 5.7 to 6.5 at 30°C temperature lift and 2.2 to 2.8 at 70°C [9].

Similarly, Frate et al. [20] reviewed the suitability of a pool of working fluids for HTHP applications. The authors considered a highest level of heat sink temperature of 150°C and a lowest level of heat source temperature of 50°C. After imposing thermodynamic, environmental, safety, and technological constraints, 27 fluids were assessed for

different operating conditions. Acetone was recommended for high heat sink and low heat source temperatures whereas benzene was recommended for high heat sink and heat source temperatures. Additionally, dichloroethane was recommended for low heat sink and high heat source temperatures. However, the latter fluids are flammable or highly flammable. On the other hand, less efficient synthetic refrigerants like R1336mzz(Z), R1234ze(Z), R1233zd(E), and R1224yd provide effective alternatives since they don't pose flammability and toxicity issues [21].

Alternatively, Bamigbetan et al. [21] evaluated different working fluids with a close approximation to a physical high temperature 20 kW heat pump with 125°C as the target heat sink temperature. Fluids R600 and R1233zd(E) were prioritized. R600 offers the compatibility with well-developed compressor technologies and flexibility. While R1233zd (E) offers a high value of COP, its stability, flammability, and safety need further testing [21]. This is also one of the fluids recommended in a novel trigeneration cycle that is still under development [19].

On the other hand, novel working fluids are being investigated for thermodynamic cycles. The latter are referred to as reactive fluids based on equilibrated chemical reactions [22,23]. Therefore, they accommodate chemical reactions and composition alterations under the influence of thermodynamic transformations. A thorough literature review has been carried out by some of the authors on the utilization of reactive working fluids in power systems [23]. However, to their knowledge, the study of reactive fluids in heat pump applications is absent in the literature.

Other heat pumps utilizing chemical reactions within the cycle are absorption HP systems (e.g. the water-ammonia system or the recently patented system based on phosphoric acid) [24–28]. However, unlike the proposed reactive heat pumps, in these systems, the chemical reactions do not directly contribute to the heat provided to the heat sink, expansion process, or heat absorbed from the heat source. In addition, these systems are generally less efficient than the conventional compressor-driven HP, and their operation is mainly limited to high source temperatures.

Therefore, taking into consideration the aforementioned gaps in the literature, this study investigates the potential of reactive fluids – rather than inert ones – in a HP system. These fluids ground on a novel energy conversion concept since they offer the advantage of the simultaneous conversion of thermal and chemical energy throughout the HP cycle, achieving by that an enhanced system performance (higher COP values compared to inert HP systems). A spectrum of equilibrated fictive reactive gaseous fluids is assessed as working fluids for an ideal HP system based on a reverse Brayton cycle. The reactive fluid's behavior in each of the HP's units is assessed and benchmarked against the behavior of comparable inert fluids. The overall performance of the reactive system is also investigated for different reaction stoichiometries and operating conditions.

2. Methods

This section describes the methodology which has been followed and introduces: the considered HP system's configuration and its application, the path followed to design the reactive fluids, the thermodynamic calculations, and the parameters at the basis of the thermodynamic assessment of the system.

Note that a similar methodology has been implemented by the authors in order to assess the performance of reactive fluids in power systems [23]. Therefore, in this study, the methodology has been adapted to heat pumps.

2.1. System configuration

The HP system used to assess the performance of gaseous reactive working fluids is comprised of a compressor, turbine, heat exchanger at the heat source side, and another heat exchanger at the heat sink side, as illustrated in Fig. 1. One should note that no phase change occurs

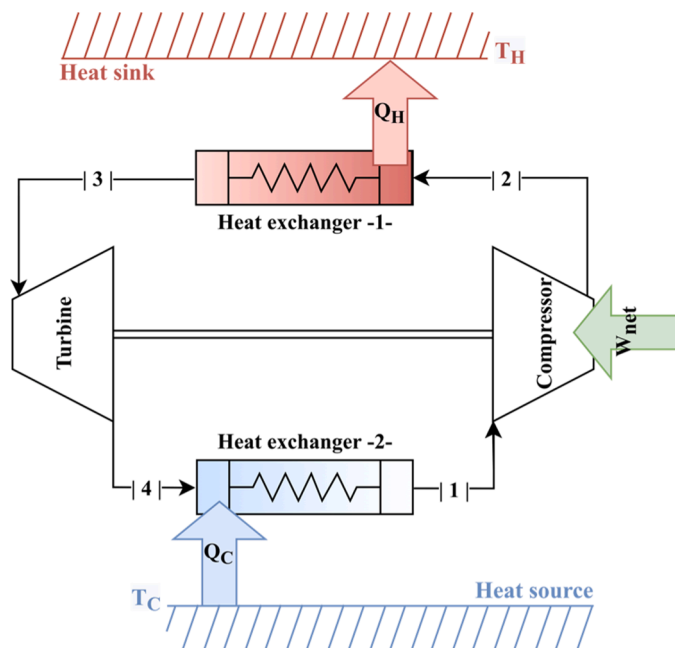


Fig. 1. The heat pump configuration considered in this study.

throughout the cycle and the fluid is considered a reactive ideal gas mixture, as detailed in Section 2.3. Therefore, this HP system represents a reverse ideal Brayton cycle. With reference to Fig. 1, the reactive fluid is compressed from point (1) to (2), then it is cooled down by rejecting heat to the heat sink (the useful effect of the HP) from point (2) to (3); this is followed by an expansion of the fluid in the turbine from point (3) to (4) and heat absorption at the heat source side. Pressure drops across the heat exchangers are neglected, and both the compressor and turbine are considered isentropic.

2.2. The design of reactive fluids

A reactive fluid is a medium that accommodates chemical reactions. Similar to the author's previous study [23], in this work, the reactions involved are assumed to occur instantaneously. This means that the reaction rapidly reaches its equilibrium state for each set of operating conditions throughout the cycle. As the fluid thermodynamic state changes when it undergoes each of the four transformations in the HP cycle, the chemical reaction shifts according to chemical equilibrium either in the exothermic or endothermic direction. This entails an altered composition of the ideal gas mixture when undergoing thermodynamic transformations.

The reactive fluid of the present study is characterized by the equilibrated single chemical equation:



where A_n and A_m are molecules made of fictive atoms "A". Parameters n and m denote the number of atoms of the molecules involved, respectively, and their values dictate the reaction stoichiometry. In this study, n is considered greater than m , and the forward direction of the reaction indicates a dissociation reaction, while the backward direction indicates an association reaction. The reactive fluids assessed are considered ideal gas mixtures of gases A_n and A_m , where the molar mass of atom A is taken to be equal to 1g/mol.

The specific heat capacity of the involved ideal gases (A_n and A_m) is assumed to be independent of temperature and defined according to the equipartition theorem [29]: the specific heat capacity of monoatomic molecules is given by $C_{p,A} = (5/2)R$, diatomic molecules $C_{p,A_2} = (7/2)R$, and polyatomic molecules $C_{p,A_k} = 4R$ (with $k > 2$), where

Table 1

Chemical reaction stoichiometric coefficients and initial number of moles.

Parameter	Value
Number of atoms of the ideal gas A_n : n	2 or 4
Number of atoms of the ideal gas A_m : m	1
Initial number of moles of A_n : $n_{A_n,0}$	1 mol
Initial number of moles of A_m : $n_{A_m,0}$	0 mol

R is the ideal gas constant. The maximum value of k considered in this study is four. These specific heat capacity values are needed to compute all the thermodynamic properties, as presented in the thermodynamic assessment section.

The spectrum of reactive fluids studied is based on ranges of the standard entropy of reaction and standard enthalpy of reaction—referred to as the reaction coordinates in this study—($\Delta_R S^\circ, \Delta_R H^\circ$), where each set of these coordinates resembles a unique reactive working fluid (unique equilibrated chemical reaction). In that matter, several points concerning the reaction coordinates need to be taken into account:

- The enthalpy change for a reaction under standard conditions ($\Delta_R H^\circ$) is positive for endothermic reactions and negative for exothermic reactions.
- The dissociation of a molecule into two or more molecules requires energy (endothermic reaction).
- For a gas-phase reaction, the entropy change of reaction under standard conditions ($\Delta_R S^\circ$) is positive when the total number of molecules of the products is greater than that of the reactants, and negative otherwise. Thus, $\Delta_R S^\circ$ is also positive for gas-phase dissociation reactions.
- If a reaction is exothermic in the forward direction, it is endothermic in the reverse direction, and vice versa. Moreover, if the entropy change is positive in the forward direction, it is negative in the opposite direction, and vice versa.

Typical values of these reaction coordinates, $\Delta_R S^\circ$ and $\Delta_R H^\circ$, fall within the ranges of 0 to 0.2 kJ/mol K for $\Delta_R S^\circ$ and 0 to 200 kJ/mol for $\Delta_R H^\circ$ [23] for the forward direction: $A_{n(g)} \rightarrow (n/m) A_{m(g)}$. Therefore,

Table 2

Thermophysical properties of the ideal gas mixture.

Property of the ideal gas mixture	Equation
Molar mass, M (g/mol)	$M = \sum_i z_i M_i$ where, z_i : molar fraction of each species i involved ($z_i = n_i/n_{tot}$) M_i : molar mass of the involved chemical species
Specific entropy, s (kJ/g K)	$s(T, P, \mathbf{z}) = (\sum_i z_i S_{i,pure}(T, P) - R \sum_i z_i \ln z_i) / M$
	$S_{i,pure}(T, P) = S_i^\circ(T_0) + C_{p,i} \ln \frac{T}{T_0} - R \ln \frac{P}{P^\circ}$
	Recall that, by definition, the standard entropy of reaction is given by: $\Delta_R S^\circ(T_0) = \sum v_i S_i^\circ(T_0)$. where, $S_{i,pure}(T, P)$: the molar entropy of the pure ideal gas i involved in the mixture (either A or A_2) $S_i^\circ(T_0)$: standard molar entropy (i.e., at $P^\circ = 1$ bar) of pure ideal gas i at temperature T_0 $C_{p,i}$: specific heat capacity of pure ideal gas i T : temperature T_0 : reference temperature (25°C) P : pressure P° : standard pressure (1 bar) v_i : stoichiometric coefficient of species i
Specific enthalpy, h (kJ/g)	$h = \sum_i z_i H_{i,pure}(T) / M$
	$H_{i,pure}(T) = \Delta_f H_i^\circ(T_0) + C_{p,i}(T - T_0)$
	Recall that, by definition, the standard enthalpy of reaction is given by: $\Delta_R H^\circ(T_0) = \sum v_i \Delta_f H_i^\circ(T_0)$. where, $H_{i,pure}(T)$: molar enthalpy of the pure ideal gas $\Delta_f H_i^\circ$: standard molar enthalpy change of formation of the ideal gas i at temperature T_0
Specific volume, v (m ³ /g)	$v = RT / PM$
Density, ρ (g/m ³)	$\rho = v^{-1}$

these are the values considered in this work.

2.3. Thermodynamic assessment

In order to determine the thermodynamic state of each point in the HP cycle, the corresponding chemical composition should be evaluated.

As described in Section 2.2, the composition of the reactive fluid throughout the cycle is governed by chemical equilibrium. From classical thermodynamics, the criterion of chemical equilibrium can be expressed as:

$$\left(\frac{dG}{d\xi} \right)_{T,P} \stackrel{chem.}{\stackrel{def.}{=} \Delta_R G} \stackrel{eq.}{=} 0 \quad \text{where} \quad \Delta_R G = \sum_i v_i \mu_i \quad (1)$$

Where G is the total Gibbs energy of the system at temperature T and pressure P [30], ξ is the extent of reaction, $\Delta_R G$ is the Gibbs-energy change of reaction, v_i is the stoichiometric coefficient of species i , and μ_i is the chemical potential of species i .

The fugacity of species i in an ideal gas mixture is equal to its partial pressure [30], so its chemical potential μ_i can be expressed as:

$$\mu_i(T, P, \mathbf{n}) = \mu_i^\circ(T) + RT \cdot \ln \left(\frac{P/P^\circ}{n_{tot}} n_i \right), \quad (2)$$

Where μ_i° is the chemical potential of pure ideal gas i at the standard pressure ($P^\circ = 1$ bar) and temperature T , n_{tot} is the total number of moles ($n_{tot} = n_{A_n} + n_{A_m}$), n_i is the number of moles of species i .

By introducing the T -dependent equilibrium constant (K_{eq}) defined as $K_{eq} = \exp \left(-\frac{\sum v_i \mu_i^\circ}{RT} \right)$, Eqs. (1) and (2) lead to:

$$K_{eq}(T) = \left(\frac{P/P^\circ}{n_{tot}} \right)^{\sum_{i=1}^{n_c} v_i} \prod_{i=1}^{n_c} n_i^{v_i}, \quad (3)$$

Where n_c is the number of different molecules forming the system. In the present case $n_c = 2$ since there are only two types of molecules – A_n and A_m – constituting the system.

Furthermore, the number of moles of each chemical species i (n_i) at temperature T and pressure P can be expressed as a function of the extent of the reaction $\xi(T, P)$, initial number of moles of the corresponding

chemical species $n_{i,0}$, and the stoichiometric coefficient v_i [30], as per Eq. (4):

$$n_i = n_{i,0} + v_i \cdot \xi(T, P). \quad (4)$$

Substituting the respective stoichiometric coefficients of the reaction in chemical Eq. (R1) ($v_{A_n} = -1$; $v_{A_m} = n/m$), number of moles representing the present chemical species (n_{A_n} ; n_{A_m}), and Eq. (4) in Eq. (3), the latter becomes,

$$K_{eq} = \left(\frac{P/P^0}{n_{A_n,0} + n_{A_m,0} + \left(\frac{n}{m}-1\right) \cdot \xi(T, P)} \right)^{\frac{n}{m}-1} \frac{(n_{A_m,0} + \frac{n}{m} \cdot \xi(T, P))^{\frac{n}{m}}}{n_{A_n,0} - \xi(T, P)}. \quad (5)$$

Moreover, the equilibrium constant K_{eq} can be evaluated as a function of the temperature (T), standard enthalpy of reaction ($\Delta_R H^0$), and standard entropy of reaction ($\Delta_R S^0$) [23,30,31] at the reference temperature T_0 (25°C), according to the Ulich approximation:

$$\ln K_{eq}(T) = \frac{\Delta_R S^0(T_0)}{R} - \frac{\Delta_R H^0(T_0)}{RT}. \quad (6)$$

Therefore, at any thermodynamic point in the HP cycle, for a given set of reaction coordinates ($\Delta_R S^0, \Delta_R H^0$) and temperature T , the equilibrium constant can be evaluated using Eq. (6). Then, substituting the stoichiometric coefficients and initial number of moles for each chemical species by their corresponding values (presented in Table 1 for this study) in Eq. (5), the extent of reaction can be evaluated at each temperature-pressure condition, $\xi(T, P)$. Knowing $\xi(T, P)$, the number of moles and molar fraction corresponding to each chemical species can be evaluated using Eq. (4), enabling the evaluation of the equilibrium composition of the reactive fluid.

All the aforementioned calculations are conducted using a Fortran code developed by the authors of this study.

Therefore, as demonstrated in Table 1, this study investigates two reaction stoichiometries, $A_{2(g)} \rightleftharpoons 2A_{(g)}$ and $A_{4(g)} \rightleftharpoons 4A_{(g)}$, for the considered ranges of reaction coordinates ($\Delta_R S^0, \Delta_R H^0$).

After determining the chemical equilibrium composition at each thermodynamic point in the cycle, knowing the corresponding pressure and temperature, the thermodynamic properties of the fluid can be evaluated following the ideal gas mixture thermodynamic model presented in Table 2 [30,32].

In this study, the heat sink (hot side) and heat source (cold side) are assumed to be at constant temperatures (T_H and T_C). These temperatures, along with the heat exchangers' pinch point temperature difference (ΔT_{pp}), are used to determine the compressor and turbine inlet temperatures (T_1 and T_3), according to the following:

$$\begin{cases} T_1 = T_C - \Delta T_{pp} \\ T_3 = T_H + \Delta T_{pp} \end{cases} \quad (14)$$

Note that the pinch point temperature difference for both of the heat exchangers is considered to be the same. Denote by ΔT_{H-C} the temperature difference $T_H - T_C$ between the heat sink and heat source. This corresponds to the actual temperature lift provided by the heat pump.

Furthermore, the system's low pressure ($P_1=P_4$) is fixed at 1 bar, as a reference value for this preliminary analysis. On the other hand, the system's high pressure ($P_2=P_3$) is varied between 5 bar and 20 bar, and the effect on the system's performance is assessed. Similarly, the system's performance is assessed for different heat source temperatures T_C (between 5°C and 50°C), difference between the heat sink and source temperatures ΔT_{H-C} (between 30°C and 100°C), and heat exchangers' pinch point temperature difference ΔT_{pp} (equal to either 5°C or 10°C) in order to observe how the HP's performance varies with the operating conditions.

Therefore, the compressor and turbine outlet temperatures (T_2 and T_4) are the only unknowns, and they can be evaluated on the basis that the compression and expansion processes are isentropic ($\Delta s = 0$). To determine these temperatures, and consequently the equilibrium

composition and other thermodynamic properties of the fluid, the equation $\Delta s = 0$ is solved between the inlet and exit of the compressor and turbine using an iterative process. The temperatures T_2 and T_4 are varied – respectively at pressures P_2 and P_4 – until the obtained entropy values, s_2 and s_4 , result to be equivalent to those at the inlet.

To assess the performance of the HP, the COP is calculated according to the equation:

$$COP = \frac{q_H}{w_{net,in}}, \quad (15)$$

Where q_H is the specific heat (specific to the mass) rejected at the heat sink heat exchanger, and it is given by the difference between the specific enthalpies at the heat exchanger's inlet (h_2) and exit (h_3) according to:

$$q_H = h_2 - h_3, \quad (16)$$

and $w_{net,in}$ is the net specific work provided to the system and is equal to the difference between the compression work (w_{comp}) and the expansion work (w_{turb}),

$$w_{net,in} = w_{comp} - w_{turb} = (h_2 - h_1) - (h_3 - h_4). \quad (17)$$

Where, h_1 and h_4 are the specific enthalpies at the compressor's inlet and turbine's exit, respectively.

In the case where, for a given reactive fluid and specific operating conditions, the heat transfer values are negative (heat flows in the opposite direction to the intended one), the system is deemed infeasible because it operates as a Brayton cycle (power cycle), instead of a reverse Brayton cycle (heat pump). Therefore, these cases are excluded from the analysis.

After assessing the performance of the reactive fluid-based HP, the latter is benchmarked against HPs operating with comparable inert gases, that are molecules A and A_2 if the reactive fluid under analysis is $A_{2(g)} \rightleftharpoons 2A_{(g)}$, or A and A_4 if the considered reaction is $A_{4(g)} \rightleftharpoons 4A_{(g)}$. The required mass flow rate, heat rejected at the heat sink, and compressor and turbine outlet temperatures of the reactive system are also compared to those of the inert ones in order to assess the technological feasibility of the system.

3. Results

This section presents the results of the methodology applied to an ideal HP cycle considering the set of operating conditions recorded in Table 3 in order to assess the behavior of reactive working fluids in a HP system. These operating conditions are arbitrary and serve the purpose of understanding how the reactive fluid behaves in each of the system's devices as a function of the reaction coordinates ($\Delta_R S^0, \Delta_R H^0$) compared to inert fluids A and A_2 . The fluid's performance is presented in Section 3.1 for the isentropic compression, Section 3.2 for the heat sink heat exchanger, and Section 3.3 for the isentropic expansion. Then, the overall reactive system performance is assessed for different reaction coordinates in Section 3.4 considering two different reaction stoichiometries. Furthermore, the effect of changing the preliminarily defined operating conditions – presented in Table 3 – on the system's

Table 3
Preliminary system operating conditions.

System operating condition	Specification
Chemical reaction	$A_{2(g)} \rightleftharpoons 2A_{(g)}$
Low pressure $P_1=P_4$	1 bar
High pressure $P_2=P_3$	5 bar
Heat source temperature T_C	10°C
Heat sink temperature T_H	50°C
Heat exchangers pinch point temperature difference ΔT_{pp}	5°C
Compressor inlet temperature $T_1=T_C-\Delta T_{pp}$	5°C
Turbine inlet temperature $T_3=T_H+\Delta T_{pp}$	55°C

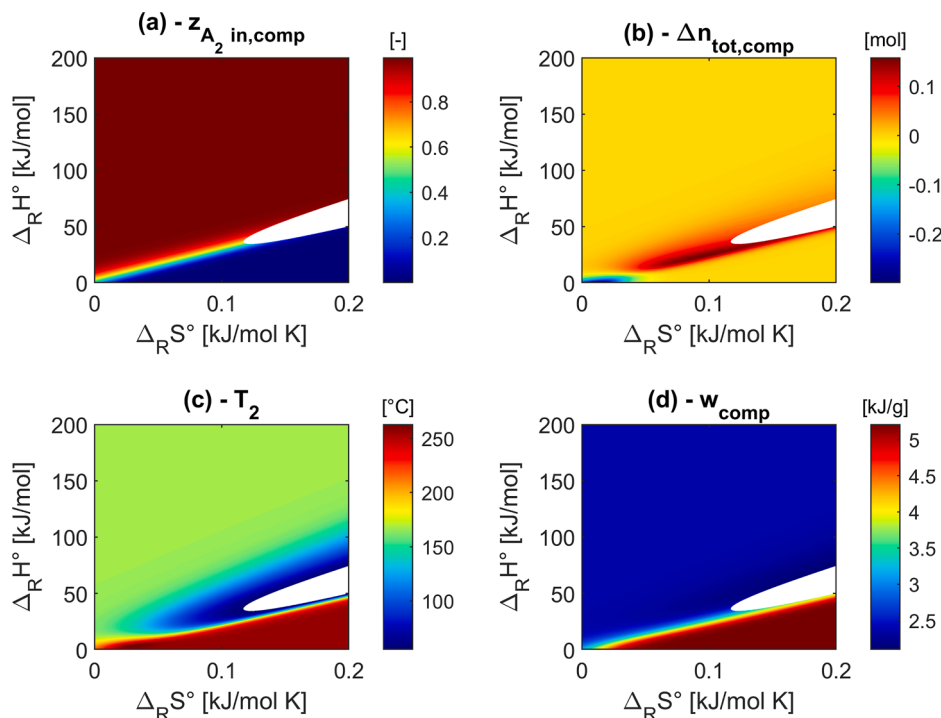


Fig. 2. Behavior of the reactive fluid ($A_{2(g)} \rightleftharpoons 2A_{(g)}$) for different reaction coordinates ($\Delta_R S^\circ$, $\Delta_R H^\circ$) under isentropic compression (from point 1→2); equilibrium molar fraction of A_2 at the compressor's inlet ($5^\circ\text{C}, 1\text{ bar}$), $z_{A_2, \text{in,comp}}$, Fig. (a); variation in the total number of moles (outlet minus inlet) of the system during compression $\Delta n_{\text{tot,comp}}$, Fig. (b); compression outlet temperature, T_2 , Fig. (c); compression specific work, w_{comp} , Fig. (d).

performance is assessed in Section 3.5. A similar discussion was performed in a previous paper [23] dedicated to power systems.

3.1. Isentropic compression

As a first step, the compression process is assessed to observe how the fluids' thermochemical characteristics ($\Delta_R S^\circ, \Delta_R H^\circ$) affect the temperature gradient in the compressor, as well as the compression work needed by the system. Thus, the equilibrium composition at the compressor's inlet ($z_{A_2, \text{in,comp}}$), the variation in the total number of moles during compression ($\Delta n_{\text{tot,comp}}$), the compressor's outlet temperature (T_2), and the specific compression work (w_{comp}) are presented in Fig. 2. In fact, $z_{A_2, \text{in,comp}}$ at the inlet of the compressor and $\Delta n_{\text{tot,comp}}$ are indicators of the reaction evolution during compression (direction and variation in the equilibrium composition).

In Fig. 2, the white zones in the colormaps represent the infeasible zones for the operation of a HP system, where the system acts as a Brayton cycle, that is as a power cycle. Indeed, heat flows in the opposite direction than the intended one. Therefore, these zones have been excluded from the analysis in this study, which is focused on heat pumps.

Fig. 2(a) presents the molar fraction at chemical equilibrium of the molecule A_2 for different reactive fluids at the compressor's inlet. It can be observed that for low values of $\Delta_R S^\circ$ and high values of $\Delta_R H^\circ$, the fluid is solely comprised of A_2 molecules (100% A_2). On the other hand, for high values of $\Delta_R S^\circ$ and low values of $\Delta_R H^\circ$, the fluid is merely composed of A molecules (100% A). This signifies that the equilibrium constant K_{eq} at the compressor's inlet is extremely low for the region of pure A_2 and high for the region of pure A . These extreme values of K_{eq} justify the regions of negligible reaction shift (negligible shift in the number of moles) during isentropic compression, as observed in Fig. 2(b). However, for intermediate values of $\Delta_R S^\circ$ and $\Delta_R H^\circ$, the compressor's inlet composition becomes highly sensitive as a function of the reaction coordinates (Fig. 2(a)), and significant variations in the total number of moles in the system result from the fluid compression (Fig. 2

(b)). Nonetheless, the reaction shifts towards the endothermic direction, characterized by an increasing number of moles ($\Delta n_{\text{tot,comp}} > 0$) for some of these intermediate values, and in the opposite, exothermic, direction ($\Delta n_{\text{tot,comp}} < 0$) for the others, as illustrated in Fig. 2(b).

The reason of the possible opposite directional shift of the reaction is related to the impact of its thermochemistry (enthalpy and entropy of reaction) and to the effects of pressure and temperature change in a compression process. If no chemical reaction occurs, the thermodynamic effect of increasing the pressure of a fluid adiabatically is that the **temperature increases**. If an equilibrated reaction occurs in a fluid, the law of mass action states that the increase of its pressure (at constant temperature) shifts the reaction in the direction dictated by the reduction of the number of moles, which is the association–**exothermic, reaction**. The exothermic reaction in an adiabatic compression, as well as the inherent inert fluid-heating process, tend to increase the temperature of the system and, thus, to shift the equilibrium in the **endothermic direction**, as dictated by the Van't Hoff equation. These are two opposite effects and the prevalence of one or the other depends on the enthalpy and entropy of reaction: when those are low, the effect of pressure on equilibrium is prevalent (exothermic reaction, $\Delta n_{\text{tot,comp}} < 0$), otherwise the effect of temperature is prevalent, and the reaction moves in the endothermic direction ($\Delta n_{\text{tot,comp}} > 0$).

Note that in the case where the fluid is composed of pure A_2 or pure A molecules, and the variation in the number of moles is negligible ($\Delta n_{\text{tot,comp}} = 0$ in Fig. 2(b)), the fluid behaves as an inert fluid in the considered transformation. Therefore, the behavior and properties of these **inert fluids**, observed at the bottom right corner (for **fluid A**) and top left corner (for **fluid A₂**) of each colormap in Fig. 2, can be used as a **benchmark to assess the behavior of reactive fluids** (intermediate values of $\Delta_R S^\circ$ and $\Delta_R H^\circ$).

From Fig. 2(c), it can be observed that for some of the reactive domain, the compressor's outlet temperature T_2 is higher – reaching a maximum of 263.8°C – compared to inert fluids A or A_2 (256.3°C for A and 167.4°C for A_2). Indeed, this reactive domain is characterized by exothermic reactions. However, this maximum outlet temperature

resulting from the reactive working fluid is comparable to that of inert fluid A_2 (3% deviation). On the other hand, for the majority of reactive fluids, T_2 is lower than that of the inert ones, and it can reach a minimum of 55°C . This means that in the case of reactive fluids, the temperature gradient during compression is much smaller compared to inert fluids. This provides more flexibility when it comes to the compressor's technology since the outlet temperature is one of the focal points in a compressor's design process. On the other hand, a sufficiently high temperature is needed at the inlet of the heat sink heat exchanger in order to reject an adequate amount of heat, which is the purpose of the HP.

Furthermore, from Fig. 2(d), it can be observed that the compression work is the highest for inert fluid A , amounting to 5.2 kJ/g . Thus, for all the considered reactive fluids, the work input required is less compared to reactive fluid A . Operating with inert fluid A_2 requires a compressor's work of 2.4 kJ/g . The reactive fluids that exhibit specific work values less than 2.4 kJ/g are characterized by the endothermic, dissociation reaction ($A_{2(g)} \rightarrow 2A_{(g)}$), as illustrated in Fig. 2(b) and Fig. 2(d), and by a low compression outlet temperature. The minimum compression work value that can be achieved by the considered reactive fluids amounts to 2.1 kJ/g . That is around 60% reduction in the compression work needed compared to fluid A , and 11% reduction compared to fluid A_2 .

Examining Fig. 2(a) and Fig. 2(d), it can be observed that the compression of inert fluid A requires more work than the compression of fluid A_2 . This is due to the fact that the molecular complexity and weight are higher for molecule A_2 , which results in the reduction of the compression work [22,33].

3.2. Heat sink side heat exchanger

Following the isentropic compression between points (1) and (2) in the HP cycle presented in Fig. 1, the fluid rejects heat into the heat sink (q_H), which is the main purpose of the system. As the amount of q_H increases, the COP also increases since both quantities are directly proportional (Eq. (15)).

The molar fraction of A_2 at the inlet of the heat exchanger ($z_{A_2, \text{in,HX1}}$),

the variation in the total number of moles between the exit and the inlet of the heat exchanger ($\Delta n_{\text{tot,HX1}}$), and the amount of specific heat rejected to the heat sink (q_H) are presented in Fig. 3.

Similar to the compressor inlet's composition presented in Fig. 2(a), the equilibrium composition of the hot side heat exchanger's inlet is pure A for high values of $\Delta_R S^\circ$ and low values of $\Delta_R H^\circ$ and pure A_2 for low values of $\Delta_R S^\circ$ and high values of $\Delta_R H^\circ$. The equilibrium composition becomes highly sensitive as a function of the reaction coordinates for the intermediate values of $\Delta_R S^\circ$ and $\Delta_R H^\circ$.

Observing Fig. 3(b), in the hot side heat exchanger where fluid's temperature is decreased at constant pressure, the reaction always shifts in the exothermic-association direction ($\Delta n_{\text{tot,HX1}} < 0$), complying with the Van't Hoff equation. This means that the reaction is in favor of the heat rejection to the heat sink. Fig. 3(a) together with Fig. 3(b) enable the assessment of the molar composition at the end of the heat exchange process. Furthermore, comparing the heat rejected by reactive fluids and non-reactive ones—presented in Fig. 3(c)—some of the reactive region (the region around the white zone) shows a very low value of heat rejected compared to inert fluids A and A_2 and the other reactive fluids. On the other hand, some of the reactive fluids exhibit values of q_H higher than those corresponding to inert fluids A and A_2 . Specifically, the highest value of q_H achieved by reactive fluids is around 4.5 kJ/g , and that is characterized by a thermochemistry that allows the maximum reduction of the number of moles. Compared to inert fluid A , this entails a 7.4% increase, and a 175% increase compared to inert fluid A_2 .

3.3. Isentropic expansion

Another factor that affects the HP's performance is the expansion work since it offsets the work required by the system.

The molar fraction of molecule A_2 at the inlet of the isentropic turbine ($z_{A_2, \text{in,turb}}$), the variation in the total number of moles during expansion ($\Delta n_{\text{tot,turb}}$), the turbine's outlet temperature (T_4), and the expansion specific work (w_{turb}) are presented in Fig. 4.

As can be observed in Fig. 4, similar conclusions can be drawn out concerning the molar composition at the turbine's inlet as the other

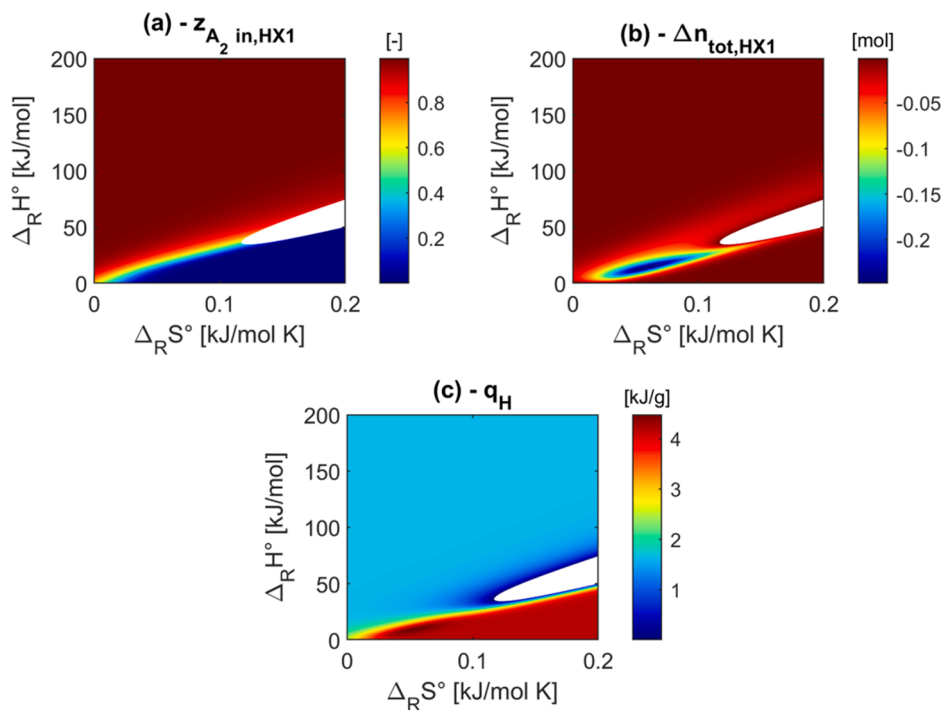


Fig. 3. Behavior of the reactive fluid ($A_{2(g)} \rightleftharpoons 2A_{(g)}$) for different reaction coordinates ($\Delta_R S^\circ$, $\Delta_R H^\circ$) in the hot-side heat exchanger (from point 2→3); equilibrium molar fraction of A_2 at the heat exchanger's inlet $z_{A_2, \text{in,HX1}}$, Fig. (a); variation in the total number of moles (outlet minus inlet) of the system during the heat exchange, $\Delta n_{\text{tot,HX1}}$, Fig. (b); specific heat rejected through the heat exchanger q_H , Fig. (c).

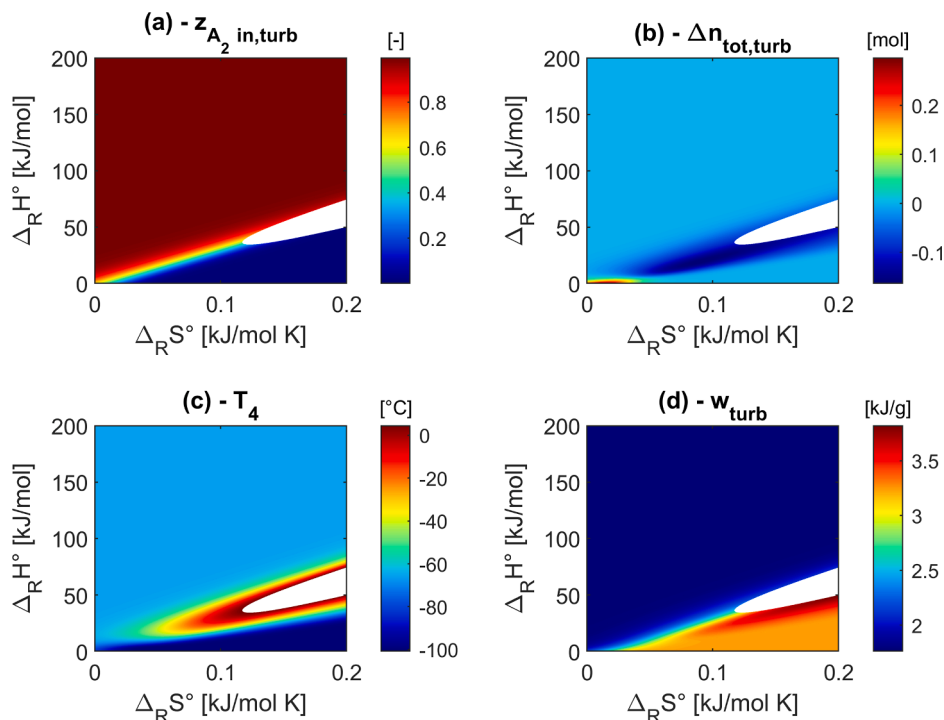


Fig. 4. Behavior of the reactive fluid ($A_{2(g)} \rightleftharpoons 2A_{(g)}$) for different reaction coordinates ($\Delta_R S^\circ$, $\Delta_R H^\circ$) under isentropic expansion (from point 3→4); equilibrium molar fraction of A_2 at the turbine's inlet (55°C, 5 bar), $z_{A_2, in, turb}$, Fig. (a); variation in the total number of moles (outlet minus inlet) of the system during expansion $\Delta n_{tot, turb}$, Fig. (b); turbine's outlet temperature, T_4 , Fig. (c); expansion specific work, w_{turb} , Fig. (d).

devices in the cycle. As in Fig. 2 and Fig. 3, also Fig. 4(a) and (b) are useful because they allow assessing the evolution of the reaction, during the expansion process, with respect to the initial compositional state.

It is observed that the majority of the reactive fluids undergo an association reaction during isentropic expansion ($\Delta n_{tot, turb} < 0$), as demonstrated in Fig. 4(b). This means that the reaction is exothermic, and the reaction shifts in the direction of decreasing number of moles.

On the contrary, observing Fig. 4(c), the temperature drop in the turbine for reactive fluids is much smaller than those corresponding to fluids A and A_2 . For inert fluid A, during expansion, the temperature drops from 55°C to around -101°C (156°C difference), and to around -66°C (121°C difference) for fluid A_2 . However, for reactive fluids, the temperature drop during expansion can reach a minimum of 50°C. This is disadvantageous to the heat transfer in the heat source heat exchanger since the higher T_4 is, less heat (q_C) can be absorbed from the heat sink.

On the other hand, Fig. 4(d) reveals that reactive fluids can generate an expansion work greater than that produced by inert fluids A and A_2 . This work can reach a maximum of 3.8 kJ/g for the considered reaction coordinates. This is 118% higher than the work produced by fluid A_2 and 18% higher than that produced by inert fluid A. Note that the highest expansion work region is characterized by a moderate association reaction ($\Delta n_{turb} < 0$).

Furthermore, as illustrated in Fig. 4(d), the expansion work produced by inert fluid A (3.2 kJ/g) is 84% greater than that produced by fluid A_2 (1.7 kJ/g). This is due to the lower molecular complexity of molecule A.

3.4. The heat pump system

In this section, the global behavior and performance of the reactive fluid in the HP system is assessed. The COP is considered as the key performance indicator of the HP system for each of the reactive fluids considered in this study. This performance is, then, benchmarked against the performance of inert fluids A and A_2 .

Therefore, the COP is defined as the ratio of the heat rejected at the heat sink side to the net work required by the HP system (Eq. (15)) and

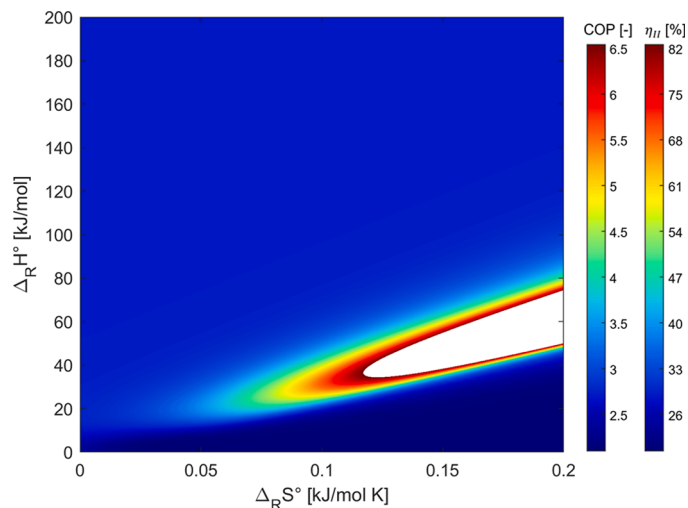


Fig. 5. Coefficient of performance (COP) and second-law efficiency (η_{II}) of the preliminary heat pump system with reaction stoichiometry $A_{2(g)} \rightleftharpoons 2A_{(g)}$ for different reaction coordinates ($\Delta_R S^\circ$, $\Delta_R H^\circ$) and the following operating conditions: $T_1=5^\circ\text{C}$, $T_3=55^\circ\text{C}$, $P_1=1$ bar, and $P_2=5$ bar.

presented in Fig. 5 for the preliminarily defined system conditions in Table 3.

Fig. 5 demonstrates that the COP that can be achieved by reactive fluids in a HP system can reach a maximum of around 6.6 for the considered ranges of reaction coordinates and operating conditions. This means an increase in the COP by a factor of around 3.1 (214% increase) compared to inert fluid A and 2.4 (144% increase) compared to A_2 for the same operating conditions. As for the second-law efficiency, defined as the COP value of the corresponding fluid against the Carnot/reversible performance of the HP system ($\eta_{II} = \text{COP}/\text{COP}_{\text{Carnot}}$), the best performing reactive fluid achieves $\eta_{II} = 80\%$ ($\eta_{II,A} = 26\%$ and $\eta_{II,A_2} = 33\%$).

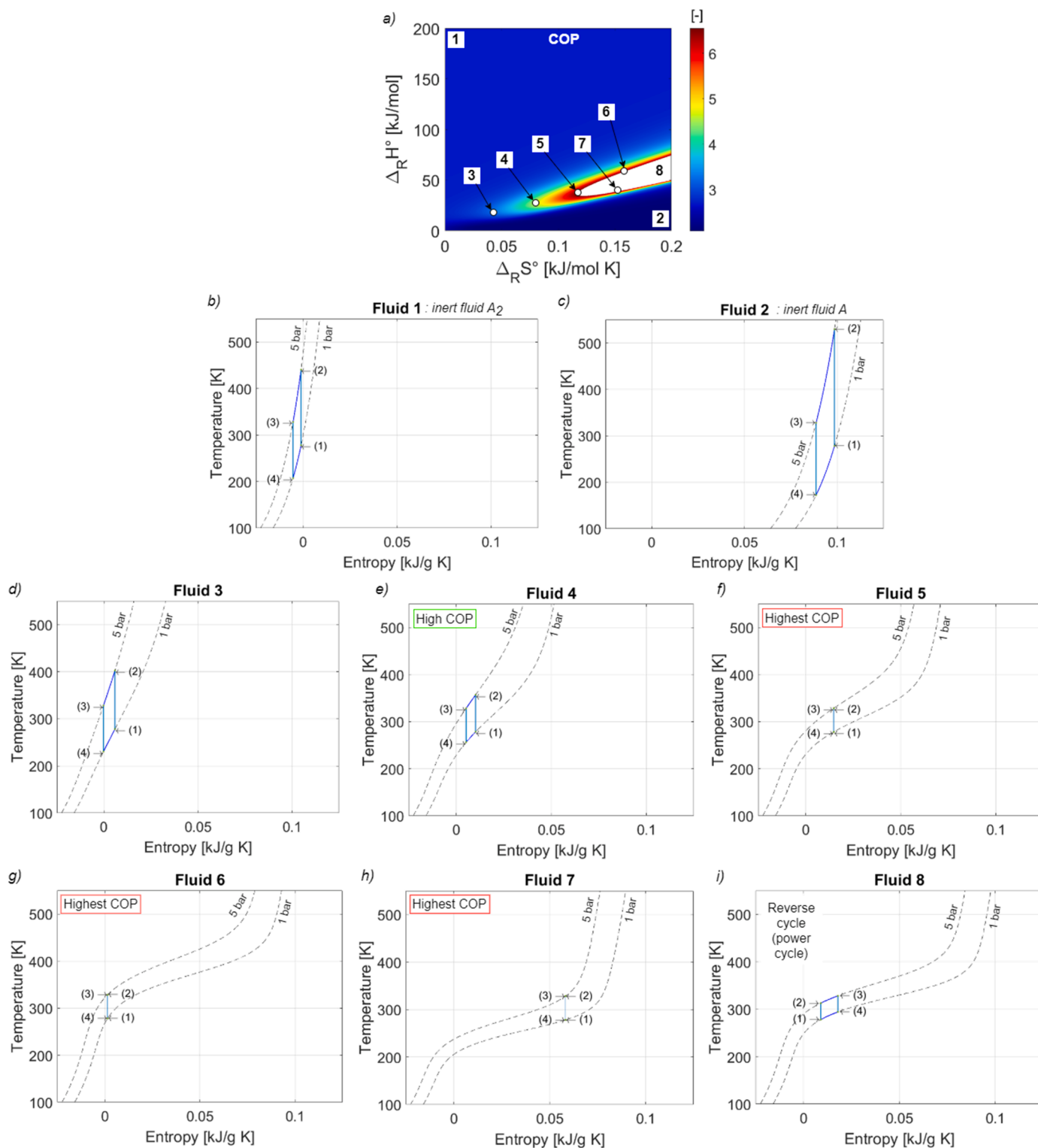


Fig. 6. T - s diagrams (Figs. (b)-(i)) of Fluids 1-8 characterized by the different reaction coordinates represented in Fig. (a) for the reaction stoichiometry $A_{2(g)} \rightleftharpoons 2A_{(g)}$ and the following operating conditions: $T_1=5^\circ\text{C}$, $T_3=55^\circ\text{C}$, $P_1=1$ bar, and $P_2=5$ bar; Figs. (b)-(i) show the two isobars at the system's high and low pressures (black dashed curves) for each of the considered Fluids 1-8. In the T - s diagrams, points (1) – (4) represent: (1) compressor's inlet; (2) compressor's outlet; (3) turbine's inlet; (4) turbine's outlet.

For completeness, it is specified that $\text{COP}_{\text{Carnot}} = T_H / (T_H - T_C) \approx 8.1$. However, the high COP region in Fig. 5 is also characterized by low values of specific heat rejected at the heat sink heat exchanger (q_H), as presented in Fig. 3(c). This means that for a certain application there is a trade-off between the HP's performance and the amount of heat

provided by the system. Additionally, if q_H is small for the highest COP values, this means the net work required by the system is also small for these reaction coordinates. In fact, for the highest COP values, the corresponding net specific work required by the system is nil, compared to around 2 kJ/g for inert fluid A and 0.6 kJ/g for A₂.

To better understand the work and heat quantities, temperature gradients, and entropy variations of the processes involved, the temperature-entropy (T - s) diagrams have been plotted in Fig. 6 for a selection of 8 sets of reaction coordinates spanning the different COP-level zones.

The selected fluids for examination are indicated on the colormap in Fig. 6(a). The corresponding T - s diagram of each of the selected 8 fluids is illustrated in Fig. 6(b) to Fig. 6(i). Fig. 6(b) and Fig. 6(c) correspond to inert fluids A_2 (Fluid 1) and A (Fluid 2), respectively. Additionally, Fig. 6(i) corresponds to the T - s diagram of a fluid (Fluid 8) that lies in the infeasible white region of the colormap.

Observing Fig. 6(a), the COP increases from reactive Fluids 3 to 7. Examining the T - s diagrams of the corresponding fluids in Fig. 6(d) to Fig. 6(h), several conclusions can be drawn. First, as the COP of the reactive fluid increases, the variation in specific entropy during heat gain and heat rejection in the two heat exchangers (between thermodynamic points (2) and (3), and (4) and (1) in the T - s diagrams) decreases, until it becomes nil for the highest COP values. Therefore, the T - s diagram would look like a vertical line or a narrow “reverse Carnot cycle” for the fluids achieving the highest COP values like Fluids 5, 6, and 7, as shown in Fig. 6(f), Fig. 6(g), and Fig. 6(h). Furthermore, as the COP achieved by a reactive fluid increases, the compressor’s outlet temperature T_2 decreases whereas the turbine’s outlet temperature T_4 increases. This can also be observed by comparing the T - s diagrams of reactive Fluids 3 and 4. Recall that the compressor’s inlet temperature T_1 and the turbines inlet temperature T_3 are fixed at 5°C and 55°C , respectively, for all the studied fluids. Hence, as the COP value increases, the corresponding fluid’s T - s diagram shrinks; the temperature gradients during compression, heat rejection, expansion, and heat absorption decrease, and the variation in entropy in the two heat exchangers also decreases.

It is noteworthy to point out that the reactive fluids characterized by the highest COP values lie at the border of the infeasible white zone. Beyond this border, lines (1-2) and (3-4) that correspond to compression and expansion, respectively, switch, and the system acts as an ideal Brayton cycle (isentropic compression, heat gain, isentropic expansion, and heat rejection). This is represented in Fig. 6(i). Although, for high COP values, the heat rejected into the heat sink decreases to almost nil (negative effect), the expansion work and compression work almost have identical values so that the expansion work compensates for the compression work, and the resulting net work required approaches zero, which is the reason behind the high COP value. On the other hand, slight differences in the COP value and temperature gradients are obtained for Fluids 5 to 7, as exhibited in Fig. 6(f)- Fig. 6(h). However, the main difference is the entropy values at the corresponding thermodynamic

points, which is dependent on the entropy of reaction relevant to the reactive fluid in question.

Given that Fig. 6(b) and Fig. 6(c) correspond to inert fluids A_2 and A (Fluids 1 and 2), the difference between these two T - s diagrams justifies why fluid A_2 achieves a higher COP value than A as a working fluid in a HP system. Analogous conclusions can be drawn by comparing the T - s diagrams of these inert fluids to the reactive ones.

Comparing the isobars in Fig. 6(b) and Fig. 6(c) that correspond to inert fluids A_2 and A , respectively, to the ones corresponding to the reactive fluids (Fig. 6(d) to Fig. 6(i)), it can be deduced that the fluid’s reactivity affects the shape of the isobars. This shape depends on the variation of the fluid’s composition, and it is responsible for the shrinking of the T - s diagram as the fluid becomes more reactive (achieving a higher COP value).

Given that the specific heat q_H results to be small for the highest performing reactive fluids, in order to achieve the same levels of thermal power, \dot{Q}_H , provided by comparable HPs operating with inert working fluids A and A_2 , several reactive HPs can be utilized in series [34,35], or the mass flow rate of the reactive fluid based HP should be increased to guarantee an equivalent thermal power $\dot{Q}_H = \dot{m} \cdot q_H$ to that of the inert fluids A and A_2 , according to Eq. (18).

$$\begin{aligned} \dot{m}_{\text{reactive}} \cdot q_{H, \text{reactive}} &= \dot{m}_A \cdot q_{H,A} \\ \text{or} & \\ \dot{m}_{\text{reactive}} \cdot q_{H, \text{reactive}} &= \dot{m}_{A_2} \cdot q_{H,A_2} \end{aligned} \quad (18)$$

In fact, each set of reaction coordinates is characterized by a COP value and the ratios of the respective fluid’s COP to that of the inert fluids ($\text{COP}_{\text{reactive}}/\text{COP}_A$ and $\text{COP}_{\text{reactive}}/\text{COP}_{A_2}$) can be evaluated accordingly. Similarly, the ratios of the reactive fluid’s mass flow rate to that of the inert fluids ($\dot{m}_{\text{reactive}}/\dot{m}_A$ and $\dot{m}_{\text{reactive}}/\dot{m}_{A_2}$) can be computed for each set of reaction coordinates according to Eq. (18). The ratios $\text{COP}_{\text{reactive}}/\text{COP}_{\text{inert}}$ and $\dot{m}_{\text{reactive}}/\dot{m}_{\text{inert}}$ can be plotted against each other in order to observe the trade-off between the required mass flow rate and the COP achieved by the cycle, as shown in Fig. 7.

Several conclusions can be drawn from Fig. 7:

- The COP value achieved by inert fluid A_2 is higher than that achieved by A . In fact, for inert fluids, the COP is only dependent on the pressure ratio of the cycle $r_p = P_2/P_1$ and the ratio $(\gamma-1)/\gamma$ where γ is the specific heat ratio C_p/C_v (the ratio of the specific heat capacity of the gas at a constant pressure to its specific heat capacity at a constant volume), according to Eq. (19):

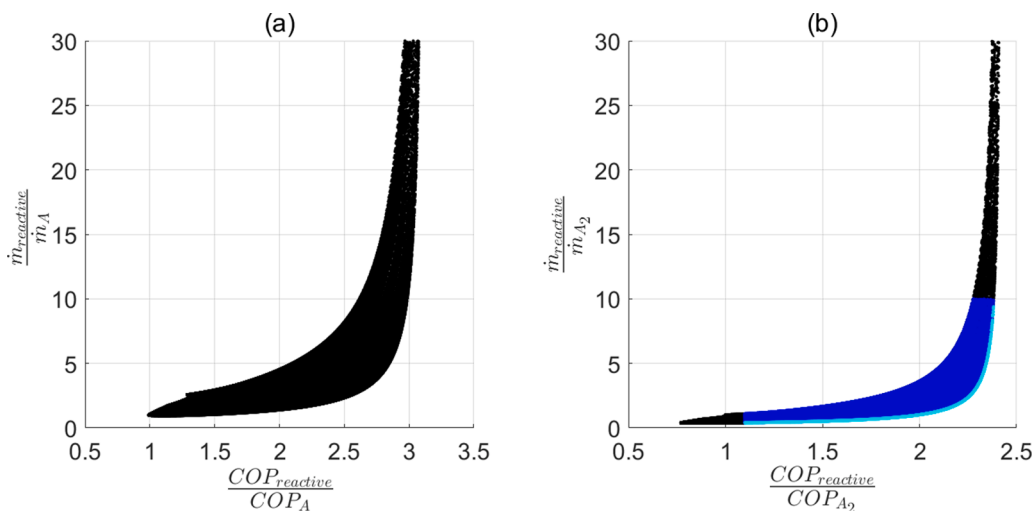


Fig. 7. Mass flow rate ratios of the studied fluids compared to inert fluids A (Fig. a) and A_2 (Fig. b) as a function of the respective COP ratios with reaction stoichiometry $A_{2(g)} \rightleftharpoons 2A_{(g)}$ for different reaction coordinates ($\Delta_R S^\circ$, $\Delta_R H^\circ$) and the following operating conditions: $T_1 = 5^\circ\text{C}$, $T_3 = 55^\circ\text{C}$, $P_1 = 1$ bar, and $P_2 = 5$ bar; suitable reactive working fluids that satisfy the conditions: $\text{COP}_{\text{reactive}}/\text{COP}_{A_2} \geq 1.1$ and $\dot{m}_{\text{reactive}}/\dot{m}_{A_2} \leq 10$ (marked in blue in Fig. (b)); selected reactive working fluids (marked in cyan in Fig. (b)).

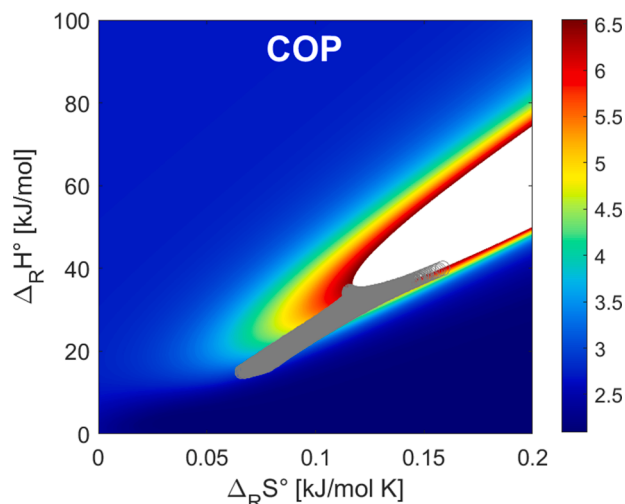


Fig. 8. Zoom on Fig. 5 with the further indication (gray empty circle mark “o”) of the potential reactive working fluids $A_{2(g)} \rightleftharpoons 2A_{1(g)}$ leading to $COP / COP_{A_2} \geq 1.1$ (COP improvement with respect to the best inert fluid, A_2) and $\dot{m} / \dot{m}_{A_2} \leq 10$ (minimum feasible mass flow rate increase required), for the studied HP system ($T_1=5^\circ\text{C}$, $T_3=55^\circ\text{C}$, $P_1=1$ bar, and $P_2=5$ bar).

$$COP_{inert} = \frac{r_p^{-1}}{r_p^{\frac{\gamma-1}{\gamma}} - 1} \quad (19)$$

Therefore, since $C_{p,A} < C_{p,A_2}$, the coefficient of performance COP_{A_2} is higher than COP_A , given that the two systems are operating with the same pressure ratio.

- As the ratio of the COP versus COP_A or COP_{A_2} increases, the mass flow rate ratios ($\dot{m}_{reactive} / \dot{m}_A$ and $\dot{m}_{reactive} / \dot{m}_{A_2}$) also increase reaching thousands for certain reaction coordinates/fluids. The reason behind these high values is the presence of a boundary in the figure separating the feasible and infeasible regions. At this boundary, the net specific work required by the system and the specific heat provided to the heat sink become negligible (Fig. 6(f), Fig. 6(g), and Fig. 6(h)), and, beyond this boundary, in the white zone, the system functions as a Brayton cycle -providing work- rather than a HP that absorbs work. However, for some fluids, also allowing an increase in COP, the mass flow rate ratio is reasonable and technologically feasible; it is also less than that required for an inert fluid system in some cases ($\dot{m}_{reactive} / \dot{m}_{inert} < 1$).

Since inert fluid A_2 is better performing than A in the heat pump system considered ($COP_{A_2} / COP_A \cong 1.3$), the reactive fluids can be

Table 4

Temperature T , pressure P , molar fraction of A_2 in the working fluid mixture z_{A_2} (in percentage), and enthalpy h at each point of the thermodynamic cycle presented in Fig. 1 for a selected reactive fluid ($\Delta_R S^\circ = 0.115$ kJ/mol K, $\Delta_R H^\circ = 30$ kJ/mol, and reaction stoichiometry $A_{2(g)} \rightleftharpoons 2A_{1(g)}$) and inert fluid A_2 as working fluids in the HP system for the following operating conditions: $T_1=5^\circ\text{C}$, $T_3=55^\circ\text{C}$, $P_1=1$ bar, and $P_2=5$ bar.

Thermodynamic point	Working fluid				Inert fluid A_2 (best comparable inert fluid)		
	Selected reactive fluid		z_{A_2} [%]	H [kJ/g]	T	P	h
	T [°C]	P [bar]			[°C]	[bar]	[kJ/g]
1	5	1	24%	8.8	5	1	4.0
2	69.5	5	14%	12.2	167.4	5	6.4
3	55	5	19%	10.7	55	5	4.8
4	-2.9	1	30%	7.5	-66	1	3.0
System's COP	5.5				2.7		
System's η_{HP}	68%				34%		

benchmarked only against fluid A_2 in order to estimate the potential performance improvements compared to the best performing inert fluid. For the considered reaction stoichiometry, operating conditions, and system configuration, the suitable reactive working fluids should guarantee an improvement in the COP against inert fluid A_2 , as well as an acceptable mass flow rate ratio $\dot{m}_{reactive} / \dot{m}_{A_2}$. In this study, a mass flow rate ratio of 10 or below is considered acceptable. Also, a minimum of 10% increase in the COP against inert fluid A_2 is considered an adequate improvement in the performance. Therefore, the region of suitable reactive fluids should provide an intersection of these two conditions ($COP_{reactive} / COP_{A_2} \geq 1.1$ and $\dot{m}_{reactive} / \dot{m}_{A_2} \leq 10$). This region of suitable reactive working fluids can be observed in Fig. 7(b) marked by a blue color. Indeed, these boundaries/conditions can be adjusted based on the application considered. However, in this blue region of Fig. 7(b), for each value of $COP_{reactive} / COP_{A_2}$, the best performing reactive fluid is the one that results in the least value of $\dot{m}_{reactive} / \dot{m}_{A_2}$ possible (least system cost and complexity). This corresponds to the lower boundary of the blue region (marked by a cyan color in Fig. 7(b)). Therefore, the reactive fluids that lie in this boundary are candidate working fluids for the heat pump system considered. Each one of these fluids are identified by a unique set of reaction coordinates, $\Delta_R S^\circ$ and $\Delta_R H^\circ$. Thus, they can be labeled on the COP colormap, previously presented in Fig. 5, with a shaded region according to Fig. 8.

The reactive fluids identified in Fig. 8 form a starting point in the process of detecting potential real – rather than fictive – reactive fluids using the corresponding ranges of reaction coordinates ($\Delta_R S^\circ, \Delta_R H^\circ$).

In order to better understand how the thermodynamic properties of the cycle vary between a reactive fluid and an inert one, a potential reactive working fluid is selected from the region shown in Fig. 8 with the following reaction coordinates: $\Delta_R S^\circ = 0.115$ kJ/mol K and $\Delta_R H^\circ = 30$ kJ/mol. The latter is compared to the better-performing inert fluid A_2 , and the thermodynamic properties at each point of the HP cycle – labelled from 1 to 4 in Fig. 1 are presented in Table 4. The mass flow rate ratio $\dot{m}_{reactive} / \dot{m}_{A_2}$ is 1.1 whereas the coefficient of performance ratio for the selected reactive fluid against A_2 ($COP_{reactive} / COP_{A_2}$) is 2.0 (103% increase in COP). For completeness, the T - s and P - h diagrams of inert gas, A_2 , and the reactive fluid selected as potential candidate are shown in Fig. 9.

The HP's performance is assessed for a different reaction stoichiometry ($A_{4(g)} \rightleftharpoons 4A_{1(g)}$) and the same operating conditions listed in Table 3. It is observed that all the considered fluids in this study (for the entire ranges of reaction coordinates) are feasible for operation in the HP system for the aforementioned stoichiometry. The corresponding compression work, expansion work, heat supplied to the heat sink, and coefficient of performance are presented in Fig. 10.

As presented in Fig. 10 for the considered ranges of reaction coordinates, it can be concluded that as the stoichiometry of the reaction changes from $A_{2(g)} \rightleftharpoons 2A_{1(g)}$ to $A_{4(g)} \rightleftharpoons 4A_{1(g)}$, the overall performance of the system with the higher stoichiometric ratio is characterized by a highest COP value of around 4.7 (Fig. 10(d)). This signifies a 124%

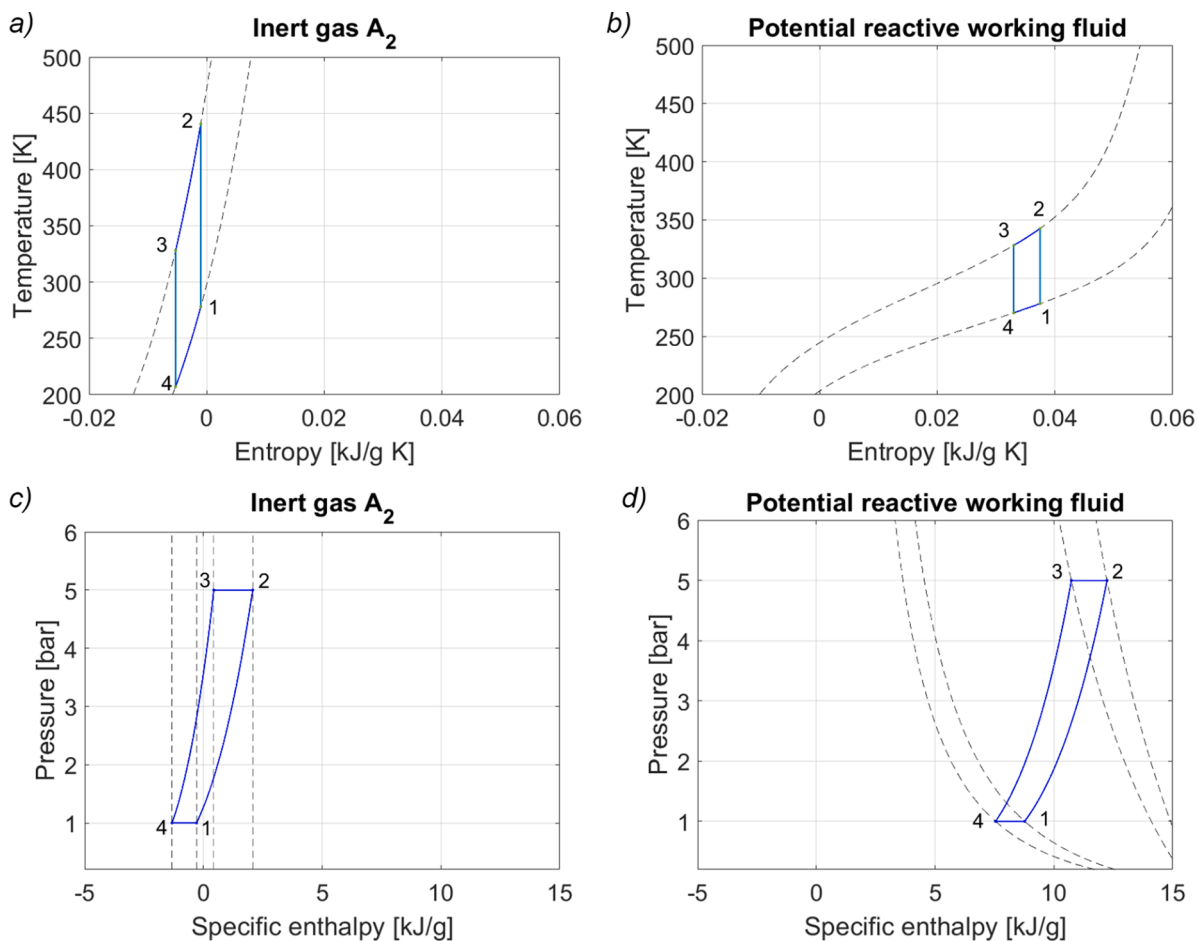


Fig. 9. T - s diagrams and P - h diagrams for the better-performing inert gas, A_2 and one of the potential working fluids $A_{2(g)} \rightleftharpoons 2A_{(g)}$ identified by $\Delta_R S^\circ = 0.115$ kJ/mol K and $\Delta_R H^\circ = 30$ kJ/mol.

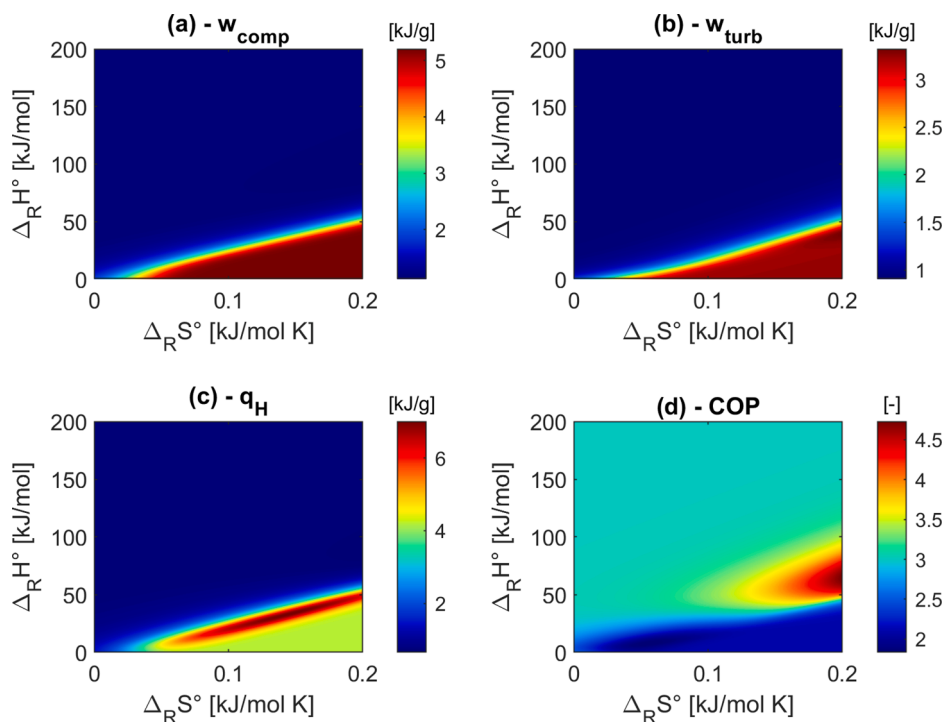


Fig. 10. Compression work, expansion work, heat supplied to the heat sink, and coefficient of performance for the different reaction coordinates ($\Delta_R S^\circ$, $\Delta_R H^\circ$) for reaction stoichiometry $A_{4(g)} \rightleftharpoons 4A_{(g)}$ and the following operating conditions: $T_1=5^\circ\text{C}$, $T_3=55^\circ\text{C}$, $P_1=1$ bar, and $P_2=5$ bar.

improvement in performance compared to a system utilizing pure fluid A, and 57% improvement compared to that of a system utilizing working fluid A₄. Therefore, the best performing reactive fluid, for the given reaction stoichiometry and operating conditions, achieves a second law efficiency $\eta_{II} = 57\%$ ($\eta_{II,A} = 26\%$ and $\eta_{II,A_4} = 37\%$). Compared to reactive fluids characterized by the reaction stoichiometry $A_{2(g)} \rightleftharpoons 2A_{(g)}$, the COP values obtained due to the stoichiometry $A_{4(g)} \rightleftharpoons 4A_{(g)}$ are lower, where the highest attainable COP is 4.7 instead of 6.6. This is due to the fact that the corresponding high COP region is characterized by lower values of q_H (Fig. 10(c)). On the other hand, the highest heat provided q_H achievable increases and reaches around 7.0 kJ/g. However, the corresponding COP value is lower than that of inert fluid A₄ and higher than that of A by around 35%.

Furthermore, evaluating the mass flow rate ratios according to Eq. (18) for the stoichiometry $A_{4(g)} \rightleftharpoons 4A_{(g)}$ results in values that do not exceed 6.4 for the ratio $\dot{m}_{reactive}/\dot{m}_A$ and 1.1 for $\dot{m}_{reactive}/\dot{m}_{A_2}$ (similar to the stoichiometry $A_{2(g)} \rightleftharpoons 2A_{(g)}$ for low and intermediate COP values, away from the boundary).

However, upon increasing the standard entropy of reaction $\Delta_R S^\circ$ from 0.2 kJ/g K to 0.4 kJ/g K (increasing the range of fluids considered in the study), an infeasible zone appears in the colormaps of the system with reaction stoichiometry $A_{4(g)} \rightleftharpoons 4A_{(g)}$. The highest COP achievable by the system increases from 4.7 (Fig. 10(d)) to around 6.6, and this value is obtained at the boundary between the feasible and infeasible regions. Furthermore, the plots of the mass flow ratios compared to inert fluids A and A₄ as a function of the COP ratios become similar to the ones displayed in Fig. 7.

3.5. System's performance as a function of the operating conditions

After assessing a preliminary HP system with the operating conditions provided in Table 3, these conditions are varied in order to evaluate their effect on the system's performance. Therefore, in this section, the effect of changing the difference between the heat sink and heat source temperatures ΔT_{H-C} , the temperature of the heat source T_C , the heat exchangers' pinch point temperature difference ΔT_{pp} , and the system's high pressure P_2 (or pressure ratio) is assessed. Note that a reaction stoichiometry of $A_{2(g)} \rightleftharpoons 2A_{(g)}$ and the reaction coordinates ranges $\Delta_R H^\circ = [0, 200]$ kJ/g and $\Delta_R S^\circ = [0, 0.2]$ kJ/g K are considered.

For a heat source temperature fixed at 5°C, system's pressure ratio at 5.0, and heat exchangers' pinch point temperature difference at 5°C, the difference between the heat source and heat sink temperatures has been varied from 30°C to 100°C in order to study its effect on the system's performance. For $\Delta T_{H-C} = 30^\circ\text{C}$, the highest COP achievable among the considered reactive fluids is 7.8, as shown in Fig. 11(a). This accounts for

a 271% increase in performance compared to inert fluid A and 189% increase compared to A₂. Note that the mass flow rate ratios ($\dot{m}_{reactive}/\dot{m}_A$ and $\dot{m}_{reactive}/\dot{m}_{A_2}$) corresponding to this best performing reactive fluid are in the order of thousands. However, as observed in Fig. 7, some other fluids with acceptable values of the mass flow ratios—offering a comparable improvement in the system's performance—can be selected. On the other hand, for $\Delta T_{H-C} = 100^\circ\text{C}$, the highest COP achievable by the reactive fluid $A_{2(g)} \rightleftharpoons 2A_{(g)}$ and the considered ranges of reaction coordinates is 3.5, as presented in Fig. 11(b). This value is 67% higher than the COP corresponding to inert fluid A and 30% higher compared to A₂. Therefore, as the temperature difference between the heat source and sink increases, the improvement in the COP of the heat pump system compared to inert fluids A and A₂ decreases. In other words, the advantage of using a reactive fluid over an inert one is more prominent for a lower value of ΔT_{H-C} . It is noteworthy to mention that varying ΔT_{H-C} does not affect the COP of inert fluids A and A₂ since the latter is only dependent on the pressure ratio and the specific heat capacities (constant for perfect gases), as demonstrated in Eq. (19). Furthermore, as ΔT_{H-C} increases, the range of potential (feasible) reactive fluids decreases (the white infeasible zone grows). Considering the second-law efficiency, for $\Delta T_{H-C} = 30^\circ\text{C}$, the best performing reactive fluid provides an improved efficiency ($\eta_{II} = 76\%$) compared to inert fluids A (20%) and A₂ (26%). Increasing ΔT_{H-C} to 100°C, the highest second-law efficiency achievable becomes $\eta_{II} = 92\%$, which is an improvement compared to inert fluid A (55%) and A₂ (71%).

On the other hand, in order to investigate the effect of changing the heat source temperature T_C on the system's performance, the COP is evaluated for a heat source temperature of 50°C and two values of ΔT_{H-C} (30°C and 100°C), similar to the results presented in Fig. 11. The rest of the operating conditions are maintained ($r_p = 5.0$ and $\Delta T_{pp} = 5^\circ\text{C}$). Observing Fig. 12(a), for a heat source temperature $T_C = 50^\circ\text{C}$ and $\Delta T_{H-C} = 30^\circ\text{C}$, the highest COP achievable by the studied reactive fluids amounts to 9.0. Thus, the corresponding reactive fluid provides a 329% performance improvement compared to inert fluid A and 233% compared to A₂. This improvement in the COP compared to the inert fluids is more prominent than the one obtained for a heat source temperature of 5°C. This can be observed by comparing Fig. 11(a) and Fig. 12(a). A similar conclusion can be drawn by comparing Fig. 11(b) and Fig. 12(b). At a higher source temperature (50°C) – for $\Delta T_{H-C} = 100^\circ\text{C}$ – the improvement in the system's performance against that of inert fluids A and A₂ is more pronounced (90% and 48%, respectively, compared to 67% and 30% at $T_C = 5^\circ\text{C}$). This improvement can be attributed to the fact that a higher heat source temperature means a higher quality and quantity of the heat absorbed by the system. Therefore, in order to provide the same amount of heat at the heat sink q_H , the system requires a lower work input. Furthermore, as demonstrated in

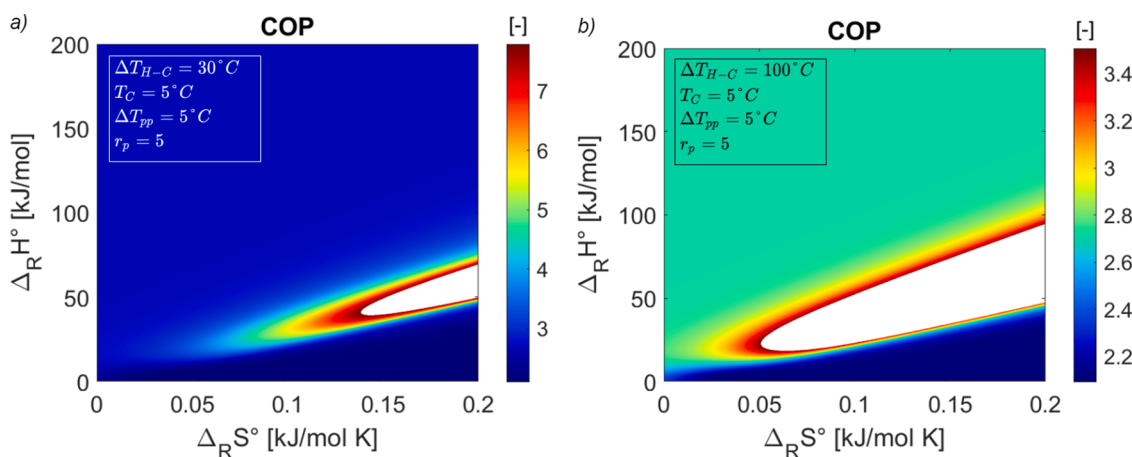


Fig. 11. Effect of the temperature difference between the heat sink and heat source on the performance of the heat pump system for reaction stoichiometry $A_{2(g)} \rightleftharpoons 2A_{(g)}$ and the following operating conditions: $T_C = 5^\circ\text{C}$, $\Delta T_{pp} = 5^\circ\text{C}$, $P_1 = 1$ bar, and $P_2 = 5$ bar.

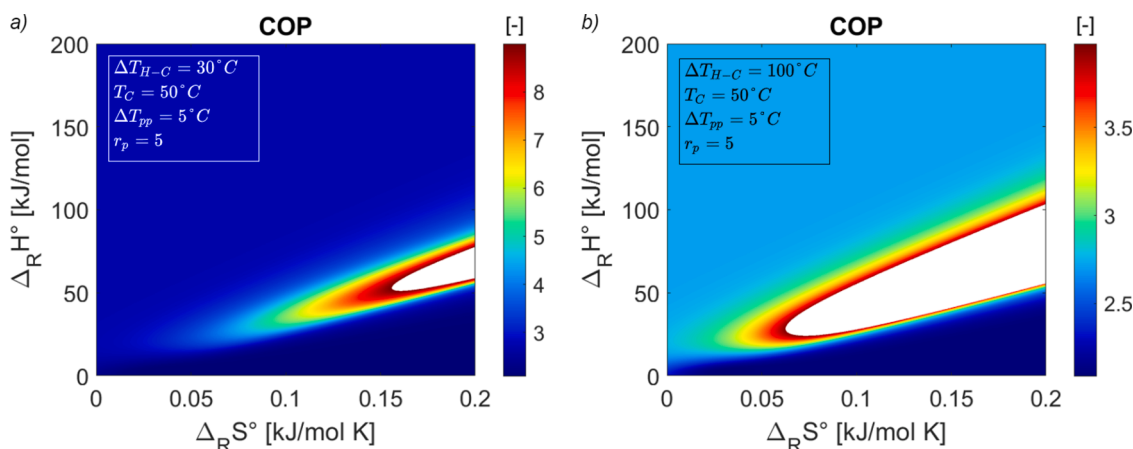


Fig. 12. System's performance for a heat source temperature 50°C and two different values of ΔT_{H-C} (30°C and 100°C) given the reaction stoichiometry $A_{2(g)} \rightleftharpoons 2A_{(g)}$ and the following operating conditions: $\Delta T_{pp}=5^\circ C$, $P_1=1$ bar, and $P_2=5$ bar.

Table 5

The studied heat pump's performance, for the three cases of operating with inert gas A, inert gas A_2 , and the best performing reactive fluid, for the considered eight sets of operating conditions, given the reaction stoichiometry $A_{2(g)} \rightleftharpoons 2A_{(g)}$.

System operating conditions			COP_{Carnot}	COP_A	COP_{A_2}	$COP_{react,max}$	$\eta_{II,A}$	η_{II,A_2}	$\eta_{II,react,max}$
ΔT_{H-C} 30°C	T_C 5°C	ΔT_{pp} 5°C	10.3	2.1	2.7	7.8	20%	26%	76%
		10°C				6.4			62%
	50°C	5°C	11.8	3.8	9.0	18%	23%	76%	
		10°C			7.3			62%	
100°C	5°C	5°C	3.8	4.2	3.5	55%	71%	92%	
		10°C						3.2	84%
	50°C	5°C	4.2	3.7	4.0	50%	64%	95%	
		10°C			3.7			88%	

Fig. 11 and Fig. 12, as the heat source temperature increases from 5°C to 50°C, the range of potential reactive working fluids also increases (the white infeasible regions in the colormaps become smaller). Concerning the second-law efficiency of the system η_{II} , the best-performing reactive fluid achieves a second law efficiency of $\eta_{II}=76\%$ for $T_C=50^\circ C$ and $\Delta T_{H-C}=30^\circ C$. This is an improvement in the performance compared to inert fluid A ($\eta_{II,A}=18\%$) and A_2 ($\eta_{II,A_2}=23\%$). Similarly, for $T_C=50^\circ C$ and $\Delta T_{H-C}=100^\circ C$, the highest η_{II} achievable among the studied reactive fluids amounts to 95%, whereas the second-law efficiency corresponding to inert fluid A is 50% and that of A_2 is 64%. Therefore, it can be concluded that as the heat source temperature increases, the improvement in the system's second-law efficiency η_{II} – due to utilizing a reactive working fluid – compared to that of inert fluids A and A_2 is amplified.

In order to assess the effect of varying the heat exchangers' pinch point temperature difference ΔT_{pp} on the system's performance compared to inert fluids A and A_2 , the COP is evaluated for four different scenarios – that are included in Table 5 – at $\Delta T_{pp}=10^\circ C$ instead of $5^\circ C$ and presented in Fig. 13. The calculations have been conducted for two different values of ΔT_{H-C} (30°C and 100°C), two different values of T_C (5°C and 50°C), and a pressure ratio $r_p=5.0$. Comparing Fig. 13(a) with Fig. 11(a), it can be observed that as ΔT_{pp} increases from 5°C to 10°C. The highest COP achievable by the system decreases from 7.8 to 6.4 (19% decrease). The reason behind the decrease in performance of the HP system is that as the pinch point temperature difference increases, the performance of the heat exchangers decreases. The same conclusion can be drawn by comparing Fig. 13(b) and Fig. 11(b), Fig. 13(c) and Fig. 12(a), and Fig. 13(d) and Fig. 12(b). However, as the temperature difference between the heat sink and source increases, the effect of varying ΔT_{pp} on the system's performance becomes less significant. For instance, for $\Delta T_{H-C}=30^\circ C$ and $T_C=5^\circ C$, increasing ΔT_{pp} from 5°C to 10°C results in a 19% reduction in the system's highest COP whereas for

$\Delta T_{H-C}=100^\circ C$ and the same heat source temperature, it results in a 9% reduction. On the other hand, for a constant value of ΔT_{H-C} , as the heat source's temperature varies, the effect of changing ΔT_{pp} on the COP is negligible. For instance, increasing ΔT_{pp} from 5°C to 10°C for $\Delta T_{H-C}=100^\circ C$ results in a comparable reduction the system's highest COP for both source temperatures 5°C and 50°C. Furthermore, comparing Fig. 11, Fig. 12, and Fig. 13, as the pinch point temperature difference increases, the range of potential reactive fluids is reduced. As for the second law efficiency COP/COP_{Carnot} the results for the studied cases are summarized in Table 5. Table 5 also summarizes the aforementioned results presented in this section for the eight sets of operating conditions.

Lastly, the system's high pressure P_2 is increased from 5 bar to 20 bar in order to observe the effect on the system's performance. Accordingly, as the system high pressure increases, the range of potential reactive fluids increases (the white infeasible zone decreases). Furthermore, the performance (COP) of the reactive fluids compared to that of inert fluids A and A_2 increases as the pressure increases. In example, for $P_2=5$ bar, the increase in COP for the best-performing reactive fluid is 271% compared to inert fluid A and 189% compared to A_2 (for $T_2=5^\circ C$, $\Delta T_{H-C}=30^\circ C$, and $\Delta T_{pp}=5^\circ C$). For the same operating conditions, with $P_2=20$ bar, the performance of the system utilizing the best performing reactive fluid becomes 343% higher than that of pure fluid A and 265% than that of A_2 . This means that the advantage of using a reactive fluid in a HP system is more prominent at higher pressures when compared to the performance of inert fluids A and A_2 . However, this conclusion cannot be generalized for the second law efficiency, COP/COP_{Carnot} , where the change in the system's η_{II} (increase/decrease) is also influenced by other operating conditions.

Therefore, for the considered reaction coordinates and reaction stoichiometry, compared to the performance of inert fluids A and A_2 , the advantage of utilizing a reactive fluid in a HP system (in terms of the COP) is more pronounced for a lower temperature difference between

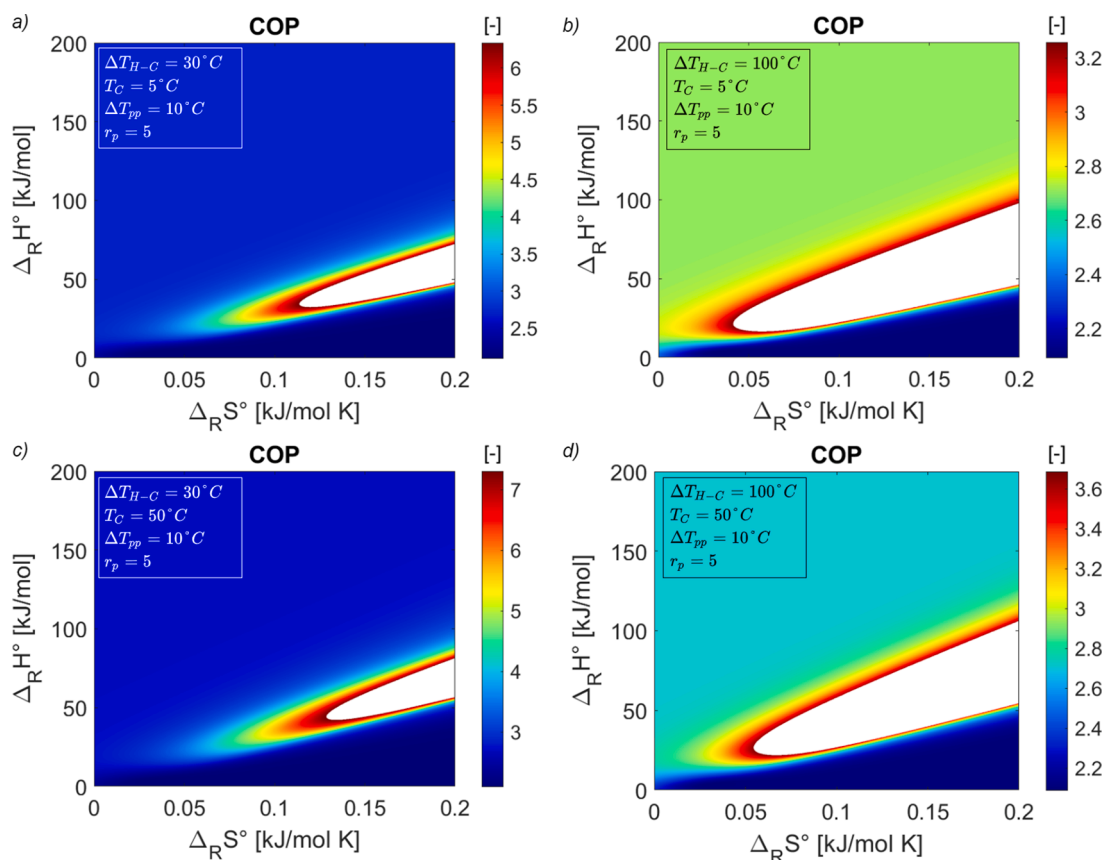


Fig. 13. System's performance for a heat exchangers' pinch point temperature difference $\Delta T_{pp}=10^\circ C$, two different values of ΔT_{H-C} ($30^\circ C$ and $100^\circ C$) and T_C ($5^\circ C$ and $50^\circ C$), pressure ratio $r_p=5$, and reaction stoichiometry $A_{2(g)} \rightleftharpoons 2A_{(g)}$.

the heat sink and source (ΔT_{H-C}), higher heat source temperature (T_C), lower heat exchangers' pinch point temperature difference (ΔT_{pp}), and higher pressure ratio.

4. Conclusion

In pursuit of assessing the potential of heat pumps operating with novel fictive reactive fluids – rather than inert ones – this work studies the performance of a spectrum of reactive fluids in each of the heat pump's devices for different operating conditions. Chemical equilibrium has been respected at each thermodynamic point in the cycle (compressor's inlet and exit and turbine's inlet and exit) in order to evaluate the chemical composition of the reactive fluid. In addition, the reactive fluid is assumed to be a mixture of ideal gases, and the heat pump system is considered ideal. Thus, the thermodynamic calculations were conducted accordingly, and two reaction stoichiometries have been considered in this study.

Results show that for the reaction stoichiometry $A_{2(g)} \rightleftharpoons 2A_{(g)}$, the coefficient of performance that can be achieved by reactive fluids in a heat pump system is 214% higher than that achieved by inert fluid A and 144% higher than that achieved by fluid A_2 . This is due to the fact that the net work required by the heat pump system significantly decreases for the highest-performing reactive fluids compared to the inert ones. However, compared to inert fluids A and A_2 , the heat provided by a heat pump system operating with the highest-performing reactive fluids to the heat sink is significantly lower. Therefore, there exists a trade-off between the system's COP and the required mass flow rate that is needed to compensate for the decrease in the heat output and ensure that the systems provide comparable thermal power. Hence, a set of criteria for selecting suitable working fluids can be defined to take into account these two parameters. In this study, a range of potential working

fluids has been identified based on the increase in the system's performance (COP) compared to that of the inert fluids and the mass flow rate required by the system in order to provide a comparable thermal power to that of the inert fluids. One of these potential reactive fluids was benchmarked against the better-performing inert fluid A_2 in order to understand how the thermodynamic properties vary due to the occurrence of equilibrated chemical reactions within the working fluid. Results show an increase by 103% in the COP compared to a system utilizing fluid A_2 where the required system's mass flow rate is only 10% higher than that needed for a system operating with inert fluid A_2 .

For a reaction stoichiometry of $A_{4(g)} \rightleftharpoons 4A_{(g)}$, the highest COP is around 124% higher than that corresponding to inert fluid A and 57% higher than that of A_4 for the considered ranges of reaction coordinates ($\Delta_R S^\circ, \Delta_R H^\circ$).

On the other hand, the performance (COP) of the reactive heat pump system—compared to that utilizing inert fluid A or A_2 —is seen to improve for a lower temperature difference between the heat sink and source, higher heat source temperature, lower heat exchangers' pinch point temperature difference, and higher pressure ratio.

As a next step, the performance of the heat pump will be assessed for real – rather than fictive – reactive fluids in order to grasp a more realistic sense of the potential gains of reactive heat pump systems.

Declaration of Competing Interest

The authors declare that they have no known competing financial interests or personal relationships that could have appeared to influence the work reported in this paper.

Data Availability

Data will be made available on request.

Funding

This research has received funding from the European Research Council (ERC) under the European Union's Horizon Europe research and innovation programme. (Grant agreement No. 101040994).

References

- [1] Heating, IEA, Paris, 2021. <https://www.iea.org/reports/heating>.
- [2] Heat Pumps, IEA, Paris, 2021. <https://www.iea.org/reports/heat-pumps>.
- [3] G. Kosmadakis, Estimating the potential of industrial (high-temperature) heat pumps for exploiting waste heat in EU industries, *Appl. Therm. Eng.* 156 (2019) 287–298, <https://doi.org/10.1016/j.applthermaleng.2019.04.082>.
- [4] D.M. van de Bor, C.A. Infante Ferreira, A.A. Kiss, Low grade waste heat recovery using heat pumps and power cycles, *Energy* 89 (2015) 864–873, <https://doi.org/10.1016/j.energy.2015.06.030>.
- [5] A. Khanlari, A. Sözen, B. Sahin, G. Di Nicola, F. Afshari, Experimental investigation on using building shower drain water as a heat source for heat pump systems. *Energy Sources, Part A: Recovery, Utilization, and Environmental Effects*, 2020, pp. 1–13, <https://doi.org/10.1080/15567036.2020.1796845>.
- [6] S. Maddah, M. Deymi-Dashtebayaz, O. Maddah, 4E analysis of thermal recovery potential of industrial wastewater in heat pumps: An invisible energy resource from the Iranian casting industry sector, *J. Clean. Prod.* 265 (2020), 121824, <https://doi.org/10.1016/j.jclepro.2020.121824>.
- [7] T. Xie, Y. Bai, J. Du, S. Kang, L. Zhao, Y. Lin, X. Wang, Air Pollution Prevention and Control Action Plan, General Office of the State Council, China, 2013. <https://policy.asiapacificenergy.org/node/2875>.
- [8] A. Nikitin, M. Deymi-Dashtebayaz, S. Muraveinikov, V. Nikitina, R. Nazeri, M. Farahnak, Comparative study of air source and ground source heat pumps in 10 coldest Russian cities based on energy-exergy-economic-environmental analysis, *J. Clean. Prod.* 321 (2021), 128979, <https://doi.org/10.1016/j.jclepro.2021.128979>.
- [9] C. Arpagaus, F. Bless, M. Uhlmann, J. Schiffmann, S.S. Bertsch, High temperature heat pumps: Market overview, state of the art, research status, refrigerants, and application potentials, *Energy* 152 (2018) 985–1010, <https://doi.org/10.1016/j.energy.2018.03.166>.
- [10] M.H. Abbasi, B. Abdullah, M.W. Ahmad, A. Rostami, J. Cullen, Heat transition in the European building sector: Overview of the heat decarbonisation practices through heat pump technology, *Sustain. Energy Technol. Assess.* 48 (2021), 101630, <https://doi.org/10.1016/j.seta.2021.101630>.
- [11] B. Zühlsdorf, J.K. Jensen, B. Elmegaard, Heat pump working fluid selection—economic and thermodynamic comparison of criteria and boundary conditions, *Int. J. Refrig.* 98 (2019) 500–513, <https://doi.org/10.1016/j.ijrefrig.2018.11.034>.
- [12] F. Afshari, A. Sözen, A. Khanlari, A.D. Tuncer, H.M. Ali, Experimental investigation of effect of refrigerant gases, compressor lubricant and operating conditions on performance of a heat pump, *J. Cent. South Univ.* 28 (2021) 3556–3568, <https://doi.org/10.1007/s11771-021-4875-7>.
- [13] M. Deymi-Dashtebayaz, A. Sulin, T. Ryabova, I. Sankina, M. Farahnak, R. Nazeri, Energy, exergoeconomic and environmental optimization of a cascade refrigeration system using different low GWP refrigerants, *J. Environ. Chem. Eng.* 9 (2021), 106473, <https://doi.org/10.1016/j.jece.2021.106473>.
- [14] F. Cao, Z. Ye, Y. Wang, Experimental investigation on the influence of internal heat exchanger in a transcritical CO₂ heat pump water heater, *Appl. Therm. Eng.* 168 (2020), 114855, <https://doi.org/10.1016/j.applthermaleng.2019.114855>.
- [15] L. Zhang, Y. Jiang, J. Dong, Y. Yao, Advances in vapor compression air source heat pump system in cold regions: A review, *Renew. Sustain. Energy Rev.* 81 (2018) 353–365, <https://doi.org/10.1016/j.rser.2017.08.009>.
- [16] Z. Wu, X. Wang, L. Sha, X. Li, X. Yang, X. Ma, Y. Zhang, Performance analysis and multi-objective optimization of the high-temperature cascade heat pump system, *Energy* 223 (2021), 120097, <https://doi.org/10.1016/j.energy.2021.120097>.
- [17] M. Deymi-Dashtebayaz, M. Rezapour, M. Farahnak, Modeling of a novel nanofluid-based concentrated photovoltaic thermal system coupled with a heat pump cycle (CPVT-HP), *Appl. Therm. Eng.* 201 (2022), 117765, <https://doi.org/10.1016/j.applthermaleng.2021.117765>.
- [18] D. Wu, B. Hu, R.Z. Wang, Vapor compression heat pumps with pure Low-GWP refrigerants, *Renew. Sustain. Energy Rev.* 138 (2021), 110571, <https://doi.org/10.1016/j.rser.2020.110571>.
- [19] A. Piña-Martinez, S. Lasala, R. Privat, V. Falk, J.-N. Jaubert, Design of Promising Working Fluids for Emergent Combined Cooling, Heating, and Power (CCHP) Systems, *ACS Sustain. Chem. Eng.* 9 (2021) 11807–11824, <https://doi.org/10.1021/acssuschemeng.1c03362>.
- [20] G.F. Frate, L. Ferrari, U. Desideri, Analysis of suitability ranges of high temperature heat pump working fluids, *Appl. Therm. Eng.* 150 (2019) 628–640, <https://doi.org/10.1016/j.applthermaleng.2019.01.034>.
- [21] O. Bamigbetan, T.M. Eikevik, P. Nekså, M. Bantle, C. Schlemminger, Theoretical analysis of suitable fluids for high temperature heat pumps up to 125°C heat delivery, *Int. J. Refrig.* 92 (2018) 185–195, <https://doi.org/10.1016/j.ijrefrig.2018.05.017>.
- [22] S. Lasala, R. Privat, J.-N. Jaubert, Inert and Reactive Working Fluids for Closed Power Cycles: Present Knowledge, Applications and Open Researches, in: E. Wang (Ed.), *Organic Rankine Cycles for Waste Heat Recovery: Analysis and Applications*, InTech, 2018.
- [23] S. Lasala, R. Privat, O. Herbinet, P. Arpentinier, D. Bonalumi, J.N. Jaubert, Thermo-chemical engines: Unexploited high-potential energy converters, *Energy Convers. Manag.* 229 (2021), 113685, <https://doi.org/10.1016/j.enconman.2020.113685>.
- [24] N. Mirf, F. Schmid, B. Bierling, K. Spindler, Design and analysis of an ammonia-water absorption heat pump, *Appl. Therm. Eng.* 165 (2020), 114531, <https://doi.org/10.1016/j.applthermaleng.2019.114531>.
- [25] M. Engler, G. Grossman, H.-M. Hellmann, Comparative simulation and investigation of ammonia-water: absorption cycles for heat pump applications, *Int. J. Refrig.* 20 (1997) 504–516, [https://doi.org/10.1016/S0140-7007\(97\)00038-8](https://doi.org/10.1016/S0140-7007(97)00038-8).
- [26] G. Manente, Y. Ding, A. Sciacovelli, Organic Rankine cycles combined with thermochemical sorption heat transformers to enhance the power output from waste heat, *Appl. Energy*. 304 (2021), 117980, <https://doi.org/10.1016/j.apenergy.2021.117980>.
- [27] V.E. Sharonov, Yu.I. Aristov, Chemical and adsorption heat pumps: Comments on the second law efficiency, *Chem. Eng. J.* 136 (2008) 419–424, <https://doi.org/10.1016/j.cej.2007.07.026>.
- [28] W. Ducheyne, C. Stevens, S. Bonte, S. Rousseau, New industrial chemical heat pump from Qpinch, 12th IEA Heat Pump Conference 2017, Rotterdam, 15–18 May.
- [29] H.B. Callen, "Thermodynamics and an Introduction to Thermostatistics". 2nd Edition, John Wiley & Sons, New York, 1960.
- [30] J.M. Smith, H.C. Van Ness, M.M. Abbott, Introduction to chemical engineering thermodynamics, McGraw-Hill, Boston, 2005, <https://doi.org/10.1021/ed027p584.3>.
- [31] U. Onken, Applied Chemical Engineering Thermodynamics, 1995, <https://doi.org/10.1002/cite.330670821>.
- [32] Y.A. Çengel, M.A. Boles, M. Kanoglu, Thermodynamics: An Engineering Approach, 9th Edition, McGraw-Hill, 2019.
- [33] E.V. Invernizzi, Prospects of Mixtures as Working Fluids in Real-Gas Brayton Cycles, *Energies*. 10 (2017) 1649, <https://doi.org/10.3390/en10101649>.
- [34] J.K. Jensen, T. Ommen, W.B. Markussen, B. Elmegaard, Design of serially connected district heating heat pumps utilising a geothermal heat source, *Energy* 137 (2017) 865–877, <https://doi.org/10.1016/j.energy.2017.03.164>.
- [35] F.R. Steward, Optimum arrangement and use of heat pumps in recovering waste heat, *Energy Convers. Manag.* 24 (1984) 123–129, [https://doi.org/10.1016/0196-8904\(84\)90023-2](https://doi.org/10.1016/0196-8904(84)90023-2).